Separation and Purification Technology 309 (2023) 122998

Contents lists available at ScienceDirect

Separation and Purification Technology

journal homepage: www.elsevier.com/locate/seppur

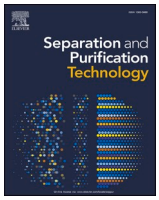

BiOX (X = I or Cl?) modified Na-$K_2Ti_6O_{13}$ nanostructured materials for efficient degradation of Tetracycline, Acid Black 1 dye and microbial disinfection in wastewater under Blue LED

Krishnakumar Balu [a,b,1,*], E. Chicardi [b], R. Sepúlveda [b], Mani Durai [a,1], Fahmida Ishaque [a,c], Deepak Chauhan [a], Young-Ho Ahn [a,*]

[a] Environmental Science and Engineering Laboratory, Department of Civil Engineering, Yeungnam University, Geongsan 38541, Republic of Korea
[b] Departamento de Ingeniería y Ciencia de los Materiales y del Transporte, E.T.S. de Ingenieros, Universidad de Sevilla, Avda. Camino de los Descubrimientos s/n, 41092 Sevilla, Spain
[c] Department of Agricultural Construction and Environmental Engineering, Sylhet Agricultural University, Sylhet 3100, Bangladesh

ARTICLE INFO

Keywords:
Blue LED
White LED
Solar light
Tetracycline
Wastewater

ABSTRACT

Photocatalysis process has emerged as a prompt method for wastewater treatment and microbial disinfection. The development of visible light active (VLA) photocatalysts, especially Blue LED active (BLA) is a challenge task for the current research scenario towards pollutants degradation and real wastewater treatment. Here, we have developed a material which is highly active under Blue LED. BiOX (X = I or Cl) modified Na-$K_2Ti_6O_{13}$ with two concentrations of BiOX was fabricated and effectively utilized for Acid Black 1 (AB 1) dye and tetracycline (TCN) degradations under Blue LED. The TCN degradation was also performed under white LED and direct solar light for comparison, and found that Na-$K_2Ti_6O_{13}$/BiOX composite was very efficient in Blue LED and white LED than direct solar irradiation. The higher activity of Na-$K_2Ti_6O_{13}$/BiOX in Blue LED confirmed by Blue light absorption of Na-$K_2Ti_6O_{13}$/BiOX *via* DRS measurements. The bare Na-$K_2Ti_6O_{13}$ is almost no active (≈10 %) under Blue LED, while Na-$K_2Ti_6O_{13}$/BiOX showed 99 % degradation under the same condition for AB 1 degradation. The stability of the Na-$K_2Ti_6O_{13}$/BiOX was tested against AB 1 dye degradation with multiple runs. The degradation intermediates of AB 1 and TCN were analysed by GC–MS, and suitable degradation pathways were proposed. The Na-$K_2Ti_6O_{13}$/BiOX was tested real wastewater treatment *via* microbial disinfection under Blue LED. The prepared composite could be effectivity used for piolet or industrial scale level effluent treatment.

1. Introduction

The globalization processes lead to competition for ingress to the fresh water, free from toxic ingredients, heavy metals, and injurious micro-organisms, and will be a vital facet for social sustainability soon [1]. At current situation, world-wide, about 1.2 billion people don't have safe intake water, and ailments spread through polluted wastewater. We are answerable for redundant infant and child deaths. Due to aquatic bacteria and intestinal viruses, there are about 502,000 diarrheal deaths happened globally [1]. Moreover, due to multidrug-resistant super-bacteria, the requirement and accessibility of hygienic and fresh water is anticipated to continue to downgrade, because of the extreme release of infective bacteria and toxic pollutants into water resources from infirmaries, industries, and bioscience/medical laboratories. Therefore, the degradation of toxic pollutants and decontamination of wastewater effluents is important to maintain an adequate water resources.

The generally used wastewater treatment methods are precipitation, adsorption, reverse osmosis, filtration and other special methods like distillation and extraction. The main disadvantage of precipitation method is sludge formation. The sludge disposal problem happened when chemical coagulation and flocculation method was adopted, since generated sludge may contain toxic substances. It was already known that the adsorption method has been used for removal of pollutants.

* Corresponding authors at: Departamento de Ingeniería y Ciencia de los Materiales y del Transporte, E.T.S. de Ingenieros, Universidad de Sevilla, Avda. Camino de los Descubrimientos s/n, 41092 Sevilla, Spain.
E-mail addresses: kbalu@us.es (K. Balu), yhahn@ynu.ac.kr (Y.-H. Ahn).
[1] These authors contributed equally to this work.

https://doi.org/10.1016/j.seppur.2022.122998
Received 5 December 2022; Received in revised form 19 December 2022; Accepted 21 December 2022
Available online 24 December 2022

However, in this method the contaminants are only transferred to the adsorbent, which need to be restored regularly, with additional costs or again becomes solid wastes. Several operational difficulties and high capital costs needed when membrane technology (ultrafiltration, nanofiltration and reverse osmosis) adopted for this purpose. Therefore, in current scenario, an alternative method is urgently needed for effective treatment of polluted wastewater.

Recently, semiconductor heterogeneous photocatalysis so called as advanced oxidation technology (AOPs) has gained attention in wastewater treatment, because of pollutants degraded completely and mineralized into non-toxic substances [2–5]. However, water disinfection/pollutant degradation by UV based (UV-A, B and C lights) irradiation results in high energy consumption method. Thus, it is essential to develop a visible active photocatalyst for cost-effective wastewater/pollutant degradation process. Using blue light radiation in LED technology offers two specific advantages: (i) It consumes lesser power, and (ii) It is more efficient in terms of light output. Unlike many costly green technologies, LEDs are accessible to the majority of individuals who want to help the environment and save money. Dyes and antibiotics, especially tetracycline (TCN), is the most basic compound in tetracycline family, and has been commonly used in human's life. By the way, TCN resistant happened, and may affect the body, and caused health problems due to its difficulty to digest. Moreover, the body only absorb 10–20 % excessive TCN, and rest directly released through biowastes (urine), to further cause water pollution. Therefore, it's a meaningful task for us to focus on tetracycline's degradation under advanced oxidation technology [6]. Xiaoli Song *et al.,* [7] reported a core shell photocatalyst titanium-organic frameworks (TPE-2NH_2@MIL-125(Ti)) for TCN degradation under visible light. In that work, on the surface of MIL-125(Ti), the ligand ((E)-4′,4‴-(1,2-diphenylethene-1,2-diyl)bis([1,1′ -biphenyl]-4-amine), TPE-2NH_2) was used. Upon visible light irradiation, about 90 % of TCN was achieved. The enhanced photocatalytic activity of the materials achieved *via* the redox state (Ti^{4+}/Ti^{3+}) and the synergism between TPE-2NH_2 and MIL-125(Ti). Direct Z-scheme $CuInS_2$/Bi_2MoO_6 heterostructure was prepared and successfully utilized for TCN dilapidation under visible light by Jingru Guo *et al.,* [8]. The performance of $CuInS_2$/Bi_2MoO_6 heterostructure activity towards TCN degradation was explained by formation of direct Z-scheme heterojunction model. Although, there were many photocatalytic systems reported for TCN degradation [8–14], most of the systems worked under UV or visible light, and the degradation TCN under LED light, especially under Blue LED is scare. Uptal Ghosh *et al.,* [15] reported TCN degradation by ultrathin g-C_3N_4 nanosheets under white LED light. It was found that, the synthesized material has about 3.3-fold higher degradation rate of TCN upon irradiation by a white LED (50 W) when compared with bulk material.

A key point to take into account is the synergistic effect of the heterostructure semiconductors on the energy levels of the electronic band structure for the complex semiconductors in order to construct reliable and effective heterojunction for the Blue LED active (BLA) photocatalyst. Constructing novel heterojunctions is an effective strategy for gaining high-performance photocatalysts [16–19]. $A_2Ti_nO_{2n+1}$ a typical general formal of titanates, and their characteristic 1D morphology (i.e. whiskers type, rods type, tubes and fibers) had been used for efficient photocatalytic processes due to their favourable electron (e^-) –hole (h^+) separation [20–27]. Among these, sodium modified potassium titanates Na-$K_2Ti_6O_{13}$ (E_{VB} ~ 2.63 eV, E_{CB} ~ −0.72 eV, Eg = 3.35 eV), the bandgap position of Na-$K_2Ti_6O_{13}$ can match flawlessly with those of pure BiOI (E_{VB} ~ +2.506 eV, E_{CB} ~ +0.346 under heterojunction − 2.06) [28] and BiOCl, because both are having strong visible light absorption.

The combination of graphitic-C_3N_4 with Na-$K_2Ti_6O_{13}$ was synthesized, characterized, and excellently used for pollutant degradation under sun and visible light reported by Qiang Wang *et al.,* [22]. The combined composite was found to be effectual photocatalytic activity when compared with individual g-C_3N_4 and Na-$K_2Ti_6O_{13}$. There is another report, potassium hexatitanate nanoparticles efficiently used for dyes (MB and RhB) degradation under UV light [25]. The potassium titanates are employed in the current research in semiconductor photolytic applications, because of its owing to their high steadiness, low rate, and harmless nature. As stated above, in order to improve its visible activity, especially under Blue LED, potassium titanate is combined with BiOI, and effectively utilized for photocatalytic degradation of antibiotic (TCN) and dye (AB 1) under Blue LED. In addition, disinfection of the total coliforms in wastewater effluent, and inactivation of the multi drug and resistant bacteria by synthesized nanocomposite was also investigated under Blue LED. The preparation of photocatalytic nanomaterials, which are significantly active in the visible light range and/or enhancing overall solar light utilization would give new momentum to photocatalytic applications since it would make possible large-scale utilization of a green source of energy i.e solar radiation. The lab scale study will be further extended to pilot/industrial scale level treatment of wastewater containing medication and toxic dyes under direct solar light.

2. Materials and methods

2.1. Chemicals used

Tetracycline (TCN), Acid Black 1 (AB 1), potassium chloride (KCl), titanium isopropoxide (TiiP), Bismuth nitrate ($Bi(NO_3)_3{\cdot}5H_2O$) pentahydrate, sodium chloride (NaCl), tetrabutylammonium iodide (TBAI), 2-propoanol, and potassium carbonate (K_2CO_3) purchased from sigma Aldrich, were used as raw materials to develop the sodium-potasium titannate (Na-$K_2Ti_6O_{13}$) and the BiOX modified Na-$K_2Ti_6O_{13}$ composites. TCN and AB 1 structures and absorption wavelengths are given in Table S1 (see Supporting information). The experimental solution was prepared using double distilled (DD) water for photocatalytic experiments. The GC–MS sample preparation details is given in supplementary file.

2.2. Instrumentations

The crystal structure of Na-$K_2Ti_6O_{13}$, Na-$K_2Ti_6O_{13}$/BiOX (I &II) and pure BIOI has been characterized by Powder X-ray diffraction (PXRD) patterns using a nickel filter CuKα radiation (30 kV, λ = 1.5419 Å, Miniflex, Rigaku, Japan) at 2θ range of 10-80°. FT-IR spectra were obtained using a Thermofisher Scientific Nicolet iS5 spectrometer. The optical properties of the sample were analyzed by UV–vis diffuse reflectance spectroscopy (UV-DRS) with Neosys-2000 instrument at 200–800 nm range. The photoluminescence study was performed using a Scinco model spectrofluorometer, Korea. FESEM was carried out on a Hitachi S-4800 at an accelerating voltage of 10 kV, the sample was prepared on an ultrasonically cleaned Si-wafer substrate, before coating, the sample was dispersed in ethanol. TEM/FE-TEM images and selected area electron diffraction (SAED) patterns were performed with an FEI-Tecnai TF-20 transmission electron microscope with an operating accelerating voltage of 120 kV. Samples for TEM were prepared by dropping sample dispersion in ethanol onto carbon-coated copper grids and letting the ethanol evaporate at room temperature. The solution of pH values was adjusted by H_2SO_4 or NaOH using a (Systronics) Digital pH meter. XPS spectra were achieved using a K-Alpha (Thermo Scientific). The non-monochromatic Al Kα line at 180–200 W was used as the primary excitation. The specific surface areas of Na-$K_2Ti_6O_{13}$ and Na-$K_2Ti_6O_{13}$/BiOX (II) was determined through nitrogen adsorption at 77 K on the basis of the BET equation using a Micromeritics ASAP 2000. For GC–MS analysis, GC–MS (QP2010 ultra, Shimadzu Co., ltd., Japan) was used.

2.3. Synthesis of Na-$K_2Ti_6O_{13}$

Initially, the synthesis of TiO_2 as the main precursor of the titanate

was prepared by a reported procedure with slight modifications [28]. Exactly, 12.5 mL of titanium isopropoxide was dissolved in 70 mL of 2-propanol. To this, 2 mL of water was added under vigorous stirring, and the stirring was continued during 3 h. After that, the formed gel was transferred to autoclave (steel) and maintain the temperature at 140 °C for 12 h. The formed product was then cooled, filtered, and washed with 1:1 ethanol (EtOH): water (H_2O) mixture, dried at 90 °C for 5 h, and ground well. The formed powder (TiO_2) was calcinated at 450 °C in muffle furnace for 5 h.

Secondly, Na-$K_2Ti_6O_{13}$ was synthesized using the molten salt method. Concretely, 1:1 mol ratio of eutectic salts (NaCl + KCl) was mixed in a mortar. After preparing eutectic salts mixture, it was mixed with K_2CO_3:TiO_2:(NaCl/KCl) (1:5.5:110 M ratio) in a mortar with a small amount of EtOH, ground for 30 min, and keep overnight. Then, they were ground again and again for 30 min, calcinated in a muffle furnace at 725 °C for 6 h, and evidently attained to room temperature. The synthesized product was well ground forcefully and treated with warm deionized water for 3 h under stirring, to remove the residual salts. Then, it was filtered and washed with EtOH, dried at 110 °C for 5 h, and followed by calcinated 450 °C for 3 h.

2.4. Fabrication of BiOI modified Na-$K_2Ti_6O_{13}$

Our primary aim is to prepare BiOI modified Na-$K_2Ti_6O_{13}$ composites, and they were prepared by solid state dispersion along with precipitation method (see Scheme S1 in supplementary information). Exactly, 1.5 g of Na-$K_2Ti_6O_{13}$ was firstly disseminated in 20 mL of ethanol. Subsequently, 10 mL of acetic acid/water mixture solution containing 0.001 M of $Bi(NO_3)_3{\cdot}5H_2O$ was added Na-$K_2Ti_6O_{13}$ dispersion under stirring condition. After that, 15 mL of alcoholic solution containing 0.001 M of TBAI was added to Na-$K_2Ti_6O_{13}$/bismuth nitrate mixture. The stirring was continued overnight, and then the catalyst was separated by filtration. The obtained mixture was with the mixture of the solvents (1:1) EtOH and water, and dried at 110 °C for 5 h. The synthesized white-orange colour precipitate Na-$K_2Ti_6O_{13}$/BiOI (I) contains 20 wt% of BiOI. The catalyst contains 32 wt% of BiOI (Na-$K_2Ti_6O_{13}$/BiOI (II)) was prepared with respective amount of bismuth nitrate and TBAI. The pure BiOI was also prepared via the reaction between $Bi(NO_3)_3{\cdot}5H_2O$ and TBAI.

2.5. Photocatalytic degradation experiments.

Photocatalytic activities towards TCN and AB1 degradation of the prepared materials were evaluated under Blue LED (50 W; emission wavelength of approximately 420–480 nm (Figure S1); 5 mW/cm^2), white LED (100 W; approximately 450–570 nm); 46 mW/cm^2)), and direct sunlight (95 mW/cm^2). Between 11 a.m and 2p.m, the solar experiments were performed (Geongsan, South Korea), and the intensity of solar light was almost constant during the experiments. In each experiment, 100 mL of the pollutants were taken (TCN-20 ppm; AB 1–10 ppm) with appropriate amount of catalyst in a beaker at dark under string condition, the adsorption–desorption equilibrium was reached in 30 min. Then, it was irradiated to the Blue and white LEDs (10 cm distance from the lamp) and direct solar light, at particular time intervals, the samples (3–4 mL) were collected, centrifuged and analyzed in UV–vis spectrometer (615 nm- AB 1; 357 nm - TCN).

2.6. Antimicrobial activities experiment under Blue LED

2.6.1. Removal of the total coliforms in wastewater effluent

The secondary effluent (SE) was obtained from a nearby municipal wastewater treatment plant (MWWTP) to estimate the total coliform (TC) following the standard total coliform membrane filtration method [29]. Firstly, 100 mL of wastewater was mixed with 10 mg of the catalyst (100 μg/mL) in a 250 mL beaker. Then the photocatalytic treatment was done by illuminating this suspension in stirred condition under Blue LED light of 5 mW/cm^2 for 2 hrs. An aliquot of 1 mL wastewater sample was collected in stipulated time intervals of 30 min and resuspended in phosphate-buffer saline (PBS) solution of pH 7.2, PBS solution as serial 10-fold dilution up to 10^{-3}. A predetermined 20 mL diluted sample was filtered through a sterile membrane filter unit and the filter paper retains the bacteria found in that sample. After that, the filter of 0.45 μm pore size (Advantec, Toyo Roshi Kaisha, ltd., Japan) was transferred to the freshly prepared petri dish of m-Endo agar and incubated at 35 ± 0.5 °C for 24 h. The petri plate of 20–80 sheen coliform colonies was counted after incubation period and total coliform was calculated per 100 mL of original sample. This experiment was repeated for dark condition with only 10 mg of the catalyst (100 g/mL of Na-$K_2Ti_6O_{13}$/BiOX (II)).

$$\text{Total coliform per 100 mL} = \left[\frac{\text{Coliform colonies counted} \times 100}{\text{mL sample filtered}}\right] \quad (1)$$

2.6.2. Disinfection of the multi drug resistant bacteria (MDRB) under Blue LED

The antimicrobial activity of the nanoparticles (Na-$K_2Ti_6O_{13}$/BiOX (II)) to control the MDR bacteria, *Enterobacter asburiae* (SC_1) was examined under Blue LED irradiation. Multi drug resistant bacteria *Enterobacter asburiae* (SC_1) was isolated from hospital waster [30]. The overnight bacterial culture of multi drug resistant bacteria *Enterobacter asburiae* (SC_1) was prepared at 37 °C using LB media at 200 rpm and a cell density of 1–2 × 10^8 CFU/mL was harvested. After that, bacteria culture with or without nanoparticles in PBS solution was irradiated with Blue LED. The viable cells evaluation was performed at 0, 30, 60, 90 and 120 min, in each time, the sample (0.1 mL) was diluted serially and spread onto LB agar and incubated at 37 °C for 24 h. Same experiment was repeated under dark condition (without Blue LED) with nanoparticles and only Blue LED (without nanoparticles) and inactivation of MDRB in terms of reduction in log CFU/mL was estimated. All the microbial experiments were repeated in triplicate.

3. Results and discussion

3.1. Primary analysis

Initially, all the synthesized materials were tested the activity against toxic pollutant degradation under Blue LED, the photocatalytic decolourization of AB 1 dye with different catalysts under Blue LED is shown in Fig. 1 a & b. Dye is not getting degraded under Blue LED. About 38 % decrease in the dye concentration occurred under dark condition when Na-$K_2Ti_6O_{13}$/BiOI (I) used, this may be due to adsorption of the dye on the surface of the catalyst. The dye was irradiated with Na-$K_2Ti_6O_{13}$/BiOI (I) and (II) gave 93 and 99 % of decolorization at 120 min, at the same condition bare Na-$K_2Ti_6O_{13}$ gave only 12 % decolorization. Both BiOI modified catalysts show efficient decolourization than bare Na-$K_2Ti_6O_{13}$ under Blue LED. Almost complete decolorization was achieved with Na-$K_2Ti_6O_{13}$/ BiOI (II), although pure BiOI gave about 89 % decolourization at 60 min, and remains unchanged up to 120 min, and not complete decolourization achieved. At different time of irradiation, the absorption spectra of AB 1 dye are shown in Fig. 1 c-f. As we can see, with respect to time, the absorbance peak at 615 nm is decreased in all the cases, and at the time of 120 min, there is no peak for AB 1 dye with Na-$K_2Ti_6O_{13}$/BiOI (II) process, whereas pure BiOI gave the peaks, and not decreased after 60 min irradiation (see circle in Fig. 1d). These spectral results indirectly proven that the formed intermediates not having the absorption of analytical wavelength of AB 1. This primary study reveals that BiOI modification with Na-$K_2Ti_6O_{13}$ enhance the catalytic activity of the composite and efficient decolourization achieved under Blue LED. To verify the Blue LED activity of the Na-$K_2Ti_6O_{13}$/ BiOI (II), the highly photostable antibiotic tetracycline (TCN) degradation was carried out under Blue LED. The Blue LED process is also compared with white LED and direct solar irradiation process.

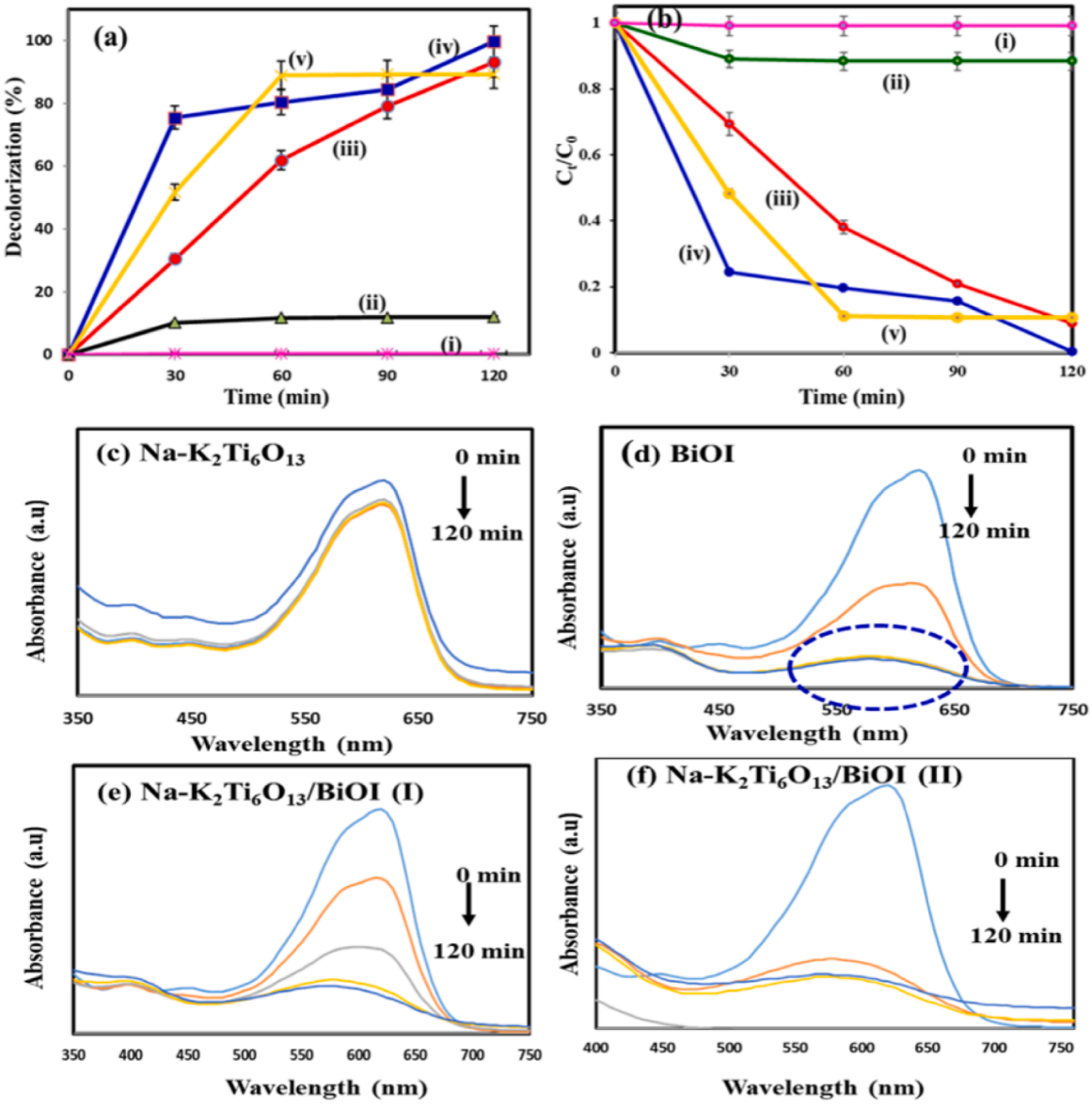

Fig. 1. Photodegradability of AB 1 under Blue LED (a) Decolorization of AB 1 with respect to time, and (b) corresponding C_t/C_0 values; (i) only Blue LED, (ii) Na-$K_2Ti_6O_{13}$ (iii) Na-$K_2Ti_6O_{13}$/BiOI (I), (iv) Na-$K_2Ti_6O_{13}$/BiOI (II), and (v) BiOI; (c-d) corresponding UV–vis spectra of the dye at different time of Blue LED irradiation, [AB 1] 10 ppm/100 mL; catalyst amount = 0.5 g/L; Blue LED = 5 mW/cm$^{2.}$ (For interpretation of the references to colour in this figure legend, the reader is referred to the web version of this article.)

3.2. *Characterization of the Na-$K_2Ti_6O_{13}$ and Na-$K_2Ti_6O_{13}$/BiOI*

Before going further applications, it is important to establish the surface characterization of the Na-$K_2Ti_6O_{13}$ and Na-$K_2Ti_6O_{13}$/BiOI. To fulfil these requirements, a complete characterization of the materials was carried out through Fourier transform infrared spectra (FT-IR), X-ray powdered diffraction (XRD), field emission scanning electron microscope (FE-SEM), Transmission electron microscopy (TEM) with elemental mapping, X-ray photoelectron spectroscopy (XPS), UV–vis diffuse reflectance spectra (DRS), Photoluminescence spectra (PL) and Brunauer, Emmett and Teller (BET) surface area measurements.

3.2.1. *XRD spectra*

XRD spectra of the synthesized bare Na-$K_2Ti_6O_{13}$, the pure BiOI and the both mixtures of Na-$K_2Ti_6O_{13}$/BiOI (I & II) are shown in the Fig. 2a-d. Firstly, for the synthesized Na modified $K_2Ti_6O_{13}$ sample (Fig. 2a), it is clearly indexed two main phases. They corresponded to the expected $K_2Ti_6O_{13}$ (ref. code no. 00–040-0403 in the PDF4 + database from ICDD). It presents monoclinic structure and *C2/m* space group symmetry. However, the peaks positions shifted to lower 2theta degree for the $K_2Ti_6O_{13}$ in comparison with the reference pattern no. 00–040-0403 can be attributable to the substitution of Na^+ by K^+ in this potassium titanate structure, obtained, finally, the Na-$K_2Ti_6O_{13}$ (Fig. S2a). This assertion is also consistent with the result of previously reported values [22,31,32]. The second main phase indexed in the Na modified $K_2Ti_6O_{13}$ sample was potassium chloride, KCl (ref. code no. 00–041-1476 in the PDF4+ database, with cubic structure and *Fm*-3m Space Group Simmetry). Although after careful washing of Na modified $K_2Ti_6O_{13}$ by warm water, the KCl salt is coming from undissolved initial salt due to the excess of K in the reaction, because K is coming from two sources, KCl and K_2CO_3 reagents.

By other hand, the XRD diagram for the synthesis of second phase for the photocatalyst material, i.e, the bismuth oxyiodide (BiOI) is showed in the Fig. 2b. There, it is clearly the formation of a main BiOI phase (ref.

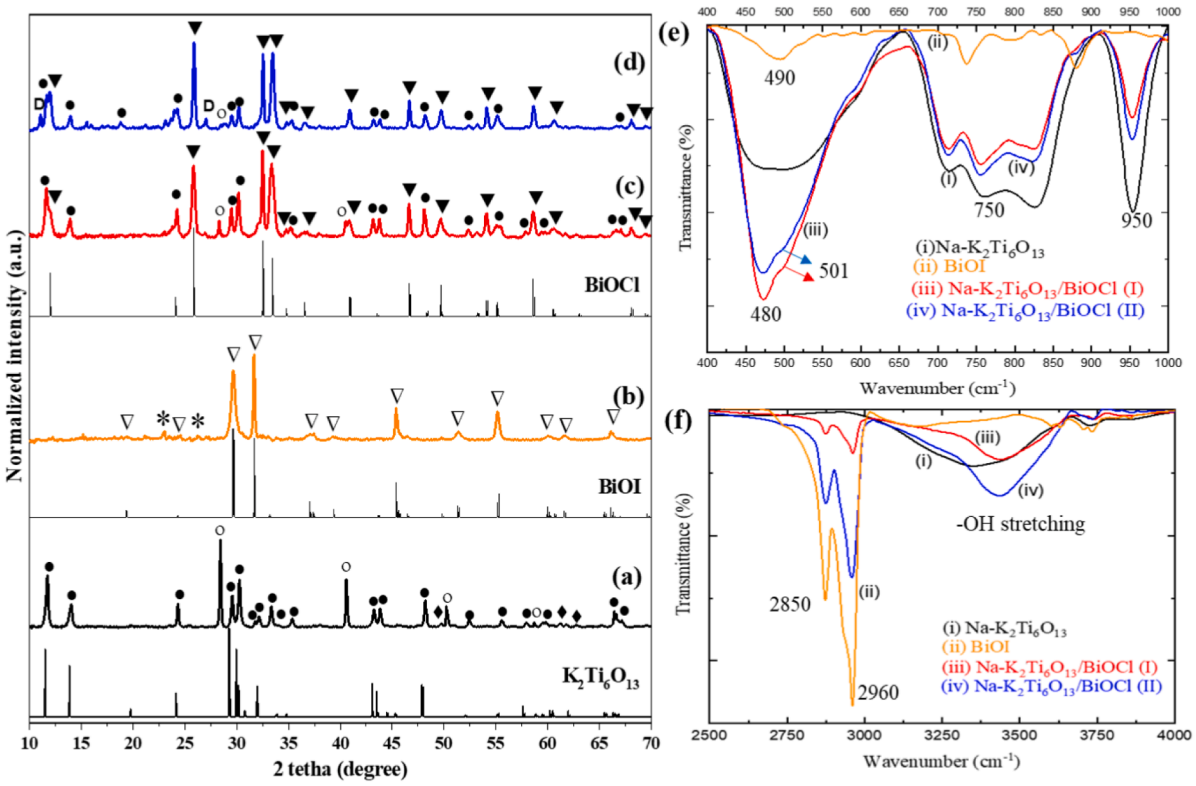

Fig. 2. XRD of (a) Na-$K_2Ti_6O_{13}$, (b) BiOI, (c) Na-$K_2Ti_6O_{13}$ /BiOX-I, (d) Na-$K_2Ti_6O_{13}$ /BiOX-II, Phases: (●) Na-$K_2Ti_6O_{13}$; (o) KCl; (▽) BiOI; (*) I_2O_5, (▼) BiOCl; (D) Na_4OI_2. For comparison purposes, it is also represented the ref. patterns corresponding to $K_2Ti_6O_{13}$, BiOI and BiOCl. FT-IR spectra of synthesised materials (e) 400 to 1000 cm^{-1} scale and (f) 2500 to 4000 cm^{-1} scale.

code no. 00–010-0445 in the database), with tetragonal structure and *P4/nmm* Space Group Symmetry), corroborating the success of the synthesis process [33,34]. Only slight peaks could be also detected, presumable corresponding to the iodine oxide (I_2O_5, ref. no. 00–022-0338 in the PDF4+ database) as sub product of the synthesis. Finally, the diffractograms for the synthesis of both BiOI modified Na-$K_2Ti_6O_{13}$ composites with different amount of BiOI (20 (I) and 32 (II) nominal wt. % of BiOI) are displayed in Fig. 2c and 2d. The most important aspect detected in both diffractograms is the main presence of the desired Na modified $K_2Ti_6O_{13}$ sample. Concretely, again the $K_2Ti_6O_{13}$ phase (ref. code no. 00–040-0403 in the PDF4+) with the peaks shifted was detected, corroborating the introduction of Na^+ in the structure of the $K_2Ti_6O_{13}$ phase. However, in this case the expected BiOI was not observed. Instead, another bismuth oxyhalide was formed, the BiOCl (Bismuth oxychloride, ref. code no. 00–006-0249 in the PDF4+ ICDD, with tetragonal structure and *P4/nmm* Space Group Symmetry). This fact can be attributable to the, before the addition of iodine source (TBAI), BiOCl was formed by the reaction between Cl (the excess KCl present in Na-$K_2Ti_6O_{13}$) and bismuth nitrate [35–38]. However, the addition of TBAI (iodine source) react with sodium and produced another orange red coloured material (may be Na_4OI_2), and which was the almost similar colour of pure BiOI (orange red colour).

Anyway, it cannot be ensuring the total absence of the I in the BiOCl, attending to the slight displacement of peaks to higher 2 theta degree, the typical displacements for BiOCl/BiOI composites (Fig. S2b) [39]. Thus, by using the fitting of the interplanar distance of the (0 0 1) and (2 0 0) crystallographic planes for the experimental BiOCl, i.e, 0.73939 nm and 0.19460 nm (lattice parameters of a = b = 0.389178 nm and c = 0.73939 nm), it can corroborated slight distortion of the z axis by comparison with the same planes for the BiOCl pattern, i.e., 0.738 nm and 0.1946 nm (a = b = 0.389178 nm and c = 0.73939 nm), suggesting the slight introduction of I (<1%) in the BiOCl structure (BiOCl/BiOI) (proved by XPS analysis, discussion comes later). Finally, in both Na-$K_2Ti_6O_{13}$/BiOCl composites (Fig. 2c and 2d) diminishing of the KCl peaks observed in comparison with the Na-$K_2Ti_6O_{13}$ specimen due to the introduction of Cl in the BiOCl structure. In addition, for the Na-$K_2Ti_6O_{13}$/BiOCl composite with higher amount of BiOCl (II), it was detected another oxyhalide phase, in this case, Na_4OI_2 (ref. cod no. 01–079-1901 in the PDF4+ ICDD, tetragonal structure and *I4/mmm* Space Group Symmetry). By other hand, the nanometric size of different phase can be corroborated using the Scherrer equation. Concretely, the Crystalline Domain Size (D) was 16.7 ± 2.7 nm for the Na-$K_2Ti_6O_{13}$. In turn, for both BiOI (Fig. 2b) and BiOCl formed (Fig. 2c and 2d), it was detected peaks with clearly different integral breadth. Thus, for the BiOI the D determined from the (1 0 2) crystallographic plane was 13.7 nm, while for the (1 1 0) was 41.3 nm. This aspect suggests a preferential crystal growth of the BiOI particles along the (1 1 0) crystallographic direction. Same behaviour can be observed in the other oxyhalide, the BiOCl, where the crystalline size were 39.2 ± 1.8 nm and 14.7 ± 2.0 nm, measured with the (1 0 0) and (1 0 2) crystallographic planes, respectively.

3.2.2. *Surface functional group analysis by IR*

FT-IR technique is good tool to discuss surface functional groups. The FT-IR spectra of layered Na-$K_2Ti_6O_{13}$, pure BiOI and the Na-$K_2Ti_6O_{13}$/BiOCl composites (I & II) were taken and the results are shown in Fig. 2 e and f and Fig. S2c and d. The band at 480 cm^{-1} in layered titanates are ascribed to O–Ti–O bending vibrations, and Ti–O stretching vibration of TiO_6 octahedral groups observed at 750 cm^{-1} (Fig. 2e). In addition, the FT-IR spectra of Na-$K_2Ti_6O_{13}$, Na-$K_2Ti_6O_{13}$/BiOCl (I & II) samples show the peak at 950 cm^{-1}corresponding to Ti = O group [40]. The –OH stretching (Fig. 2f) (between 3300 and 3500 cm^{-1}) and bending (Fig. S2d)(1600 and 1650 cm^{-1}) vibrations are observed in Na-$K_2Ti_6O_{13}$, Na-$K_2Ti_6O_{13}$/BiOCl (I & II) samples. In pure BiOI, the peak at

490 is assigned to Bi–O stretching mode. Two more peaks were observed at 1380 (asymmetry) and 1490 (symmetry) cm^{-1} for Bi–I (Fig. S2d) [41]. The strong peaks at 2850 and 2960 cm^{-1} are attributed to stretching vibration of N—C—H group in pure BiOI (Fig. 2f), and these peaks are reflected in $K_2Ti_6O_{13}$/BiOCl (I & II) samples due to residual BiOI, and Na_4OI_2, and the N—C—H group may obtain from residual TBAI which was the source of iodine in the preparation of BiOI. In $K_2Ti_6O_{13}$/BiOCl (I & II) composites the peak at 501 cm^{-1} was assigned to Bi–O stretching mode of BiOCl, the Bi-O structing mode of BiOCl was observed slightly higher wavenumber when compared with Bi-O structing mode of BiOI [42].

3.2.3. *FE-SEM, HR-TEM, and mapping of elements*

The surface morphology of the pure Na-$K_2Ti_6O_{13}$ and Na-$K_2Ti_6O_{13}$/BiOCl (II) was analysed by FE-SEM. The images of pure Na-$K_2Ti_6O_{13}$ at different magnification (Fig. S3 a and b) revealed the formation of bundles of nanobelts. After modification with BiOCl, for the Na-$K_2Ti_6O_{13}$/BiOCl (II), the surface of nanobelts become smooth due to formation of BiOCl layer (Fig. S3c and d). The morphology of Na-$K_2Ti_6O_{13}$ and Na-$K_2Ti_6O_{13}$/BiOCl (II) was further analysed by HR-TEM measurements. The TEM images of both materials at different magnification and in different locations are given in Fig. 3 along with their fingerprint regions Fig. 3 c and f. The Fig. 3a, b, and g-i show a typical TEM image of the obtained Na-$K_2Ti_6O_{13}$ nanobelts. The nanobelts/rods are almost uniform with a diameter of 60–100 nm, and several hundred nm in length (Fig. 3g-i). After modification with BiOCl, two different phases were clearly seen in the images (Fig. 3d and j). A bundle of nanosized BiOCl particles (see circles) were presented on the Na-$K_2Ti_6O_{13}$ nanobelts. The BiOCl bundles uniformly coated on the different spaces of nanobelts. The elemental composition of Na-$K_2Ti_6O_{13}$/BiOCl (II) was confirmed the formation of BiOCl rather BiOI. The Fig. 4 shows the elemental mapping of Na-$K_2Ti_6O_{13}$/BiOCl (II), and the results reflect each element present in the materials. Concretely, the elemental mapping study confirms the presence of Na, K, Ti and O in the nanobelts, corresponding to the Na-$K_2Ti_6O_{13}$. In addition, the Bi, Cl and O are also clearly detected in the area marked with a dotted white square in Fig. 4, revealing therefore to the formation of BiOCl compound instead of BiOI. So, the formed compound was BiOCl. However, the iodine (I) is present in the whole composite as another type of compound such as Na_4OI_2.

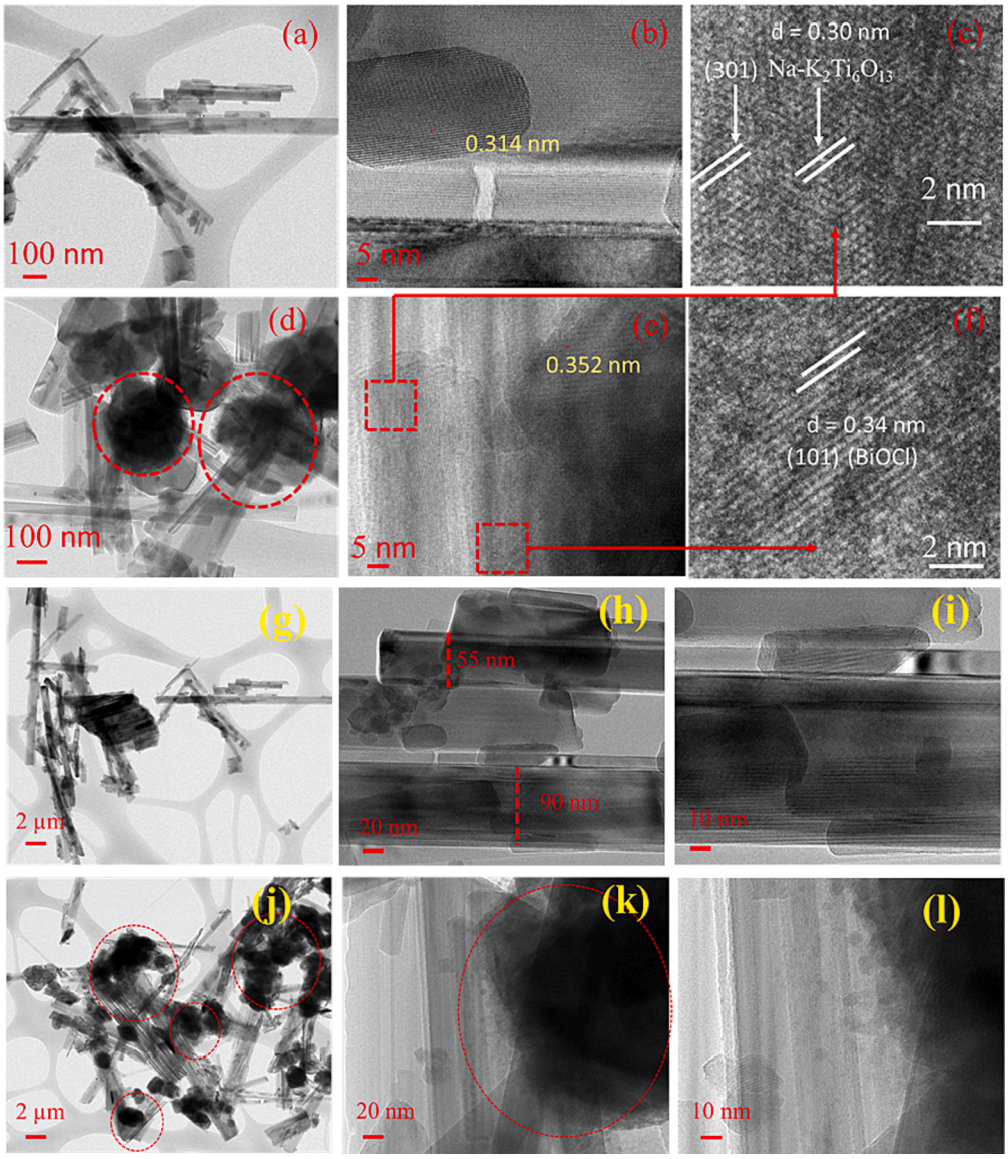

Fig. 3. HR-TEM images of Na-$K_2Ti_6O_{13}$ (a, b, g-i) and Na-$K_2Ti_6O_{13}$/BiOCl (II) (d, e, j-l) and fingerprint of Na-$K_2Ti_6O_{13}$ (c) and BiOCl (f).

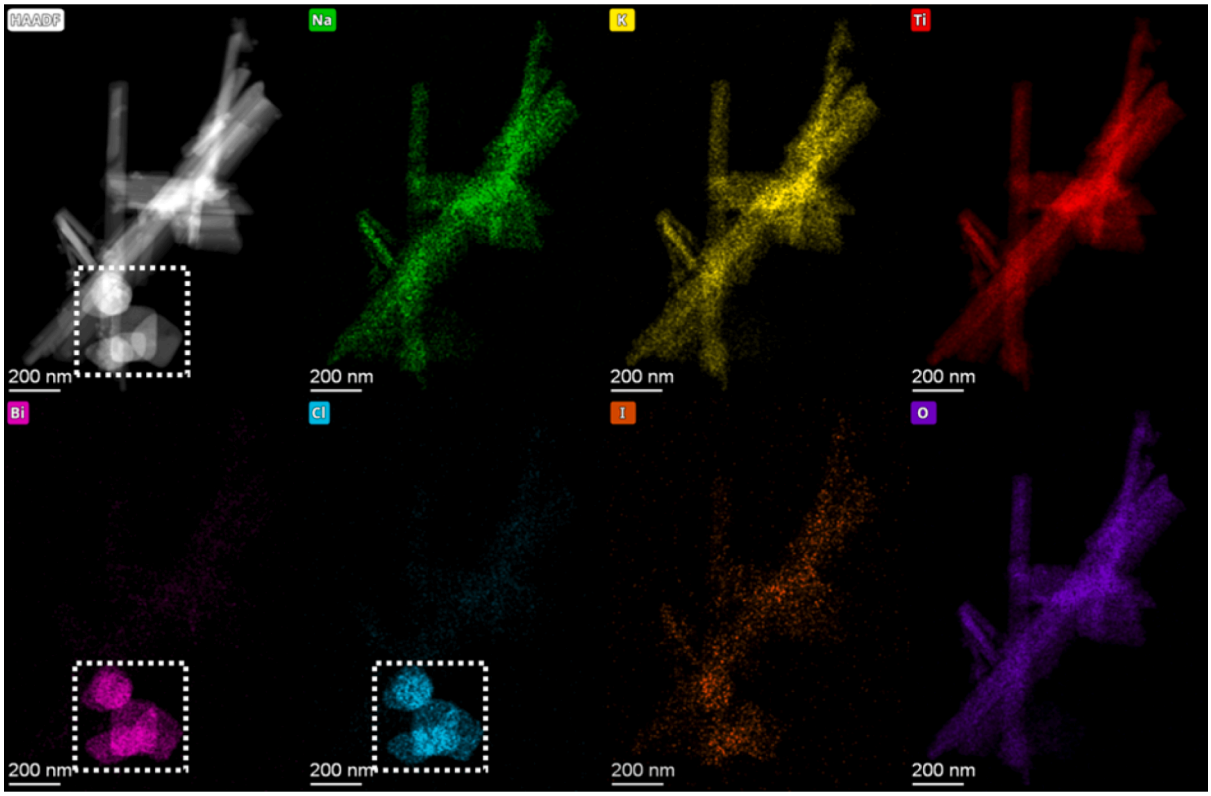

Fig. 4. Elemental mapping of a group of particles of the Na-$K_2Ti_6O_{13}$/BiOCl (II). HAADF: High-Angle Annular Dark Field image. Green; Na; Yellow: K; Red: Ti; Pink: Bi; Light blue: Cl; Orange: I; Purple: O. The dotted white square showed the group of BiOCl particles. (For interpretation of the references to colour in this figure legend, the reader is referred to the web version of this article.)

3.2.4. *XPS analysis*

In order to determine the surface oxidation state of the each materials, a X-ray photoelectron spectroscopy (XPS) measurements was performed. Fig. 5a shows that survey spectrum of Na-$K_2Ti_6O_{13}$/BiOCl (II), and shows that presence of Ti 2p, O 1 s, Bi 4f, Cl 2p, K 2p, Na 1 s, and also I 3d. The individual peaks of each element are shown in Fig. 5 (b-h). The Ti $2p_{3/2}$, and Ti $2p_{1/2}$ peaks of Ti^{4+} were observed at 458.2 eV and 464.1 eV, respectively, the reported Ti $2p_{3/2}$ peak of pure TiO_2 was 458.5 eV [43]. The B.E of O1s is observed at 529.4 eV (Bi-O) [44–46] and 531.0 eV (lattice oxygen (O_L) of TiO_2) (Fig. 5c). The Bi 4f spectrum of BiOCl in Na-$K_2Ti_6O_{13}$/BiOCl (II) exhibits two distinct peaks at 159.4 and 164.7 eV, which are corresponding to Bi $4f_{7/2}$ and Bi $4f_{5/2}$ of $[Bi_2O_2]^{2+}$, respectively [47] and belongs to Bi^{3+} in BiOCl (Fig. 5d). Significantly, upon deconvolution of the Bi 4f peak, produced two

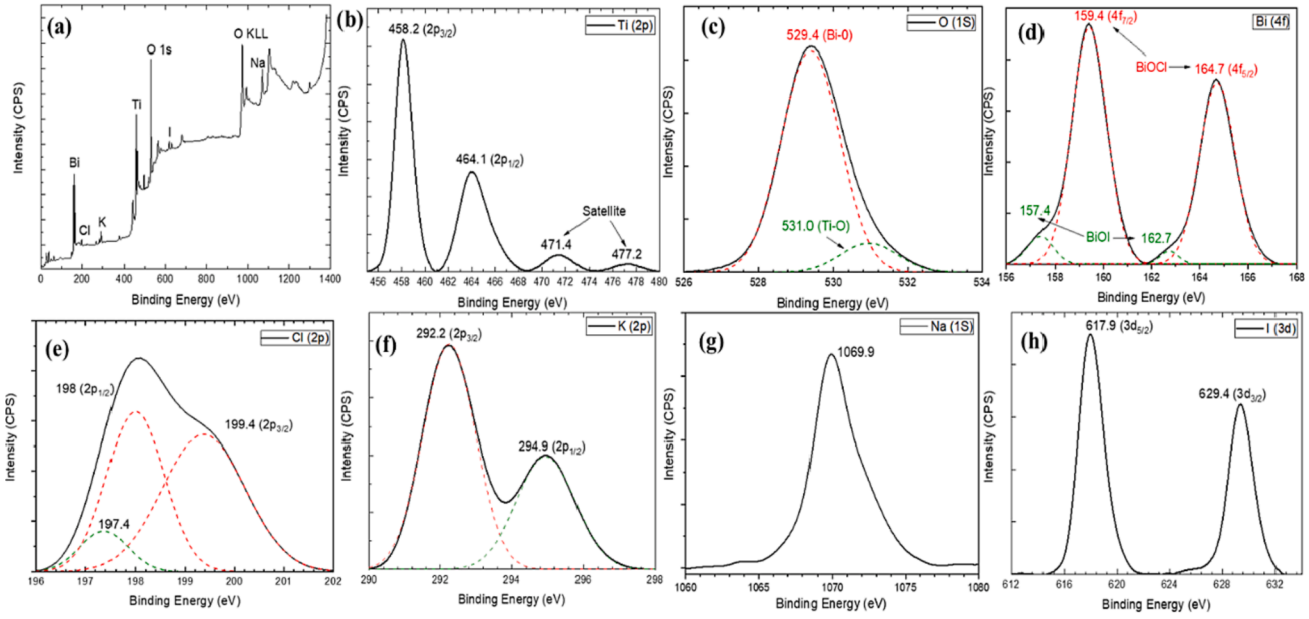

Fig. 5. XPS of Na-$K_2Ti_6O_{13}$/BiOCl (II), (a) Survey spectrum, (b) Ti 2p, (c) O 1 s, (d) Bi 4f, (e)Cl 2p, (f) K 2p (g) Na 1 s and (h) I 3d.

distinct peaks at 157.4 eV and 162.2 eV corresponding to Bi $4f_{7/2}$ and Bi $4f_{5/2}$ of BiOI [46,48], respectively, which confirm that a little amount of Cl displacement by I in Na-$K_2Ti_6O_{13}$/BiOCl (II). The asymmetric Cl 2p spectrum is fitted with two peaks at 198.0 eV and 199.4 eV (Fig. 5e), which can be indexed to the $2p_{1/2}$ and $2p_{3/2}$ of Cl in BiOCl [46]. Upon deconvolution, a small peak appeared at 197.4 eV ($2p_{1/2}$) (Fig. 5e) corresponding to Cl present in residual KCl [49]. The K binding energy peaks were observed at 292.2 ($2p_{3/2}$) and 294.9 eV ($2p_{1/2}$) [50], and these values are exactly matching with the K present in $K_2Ti_6O_{13}$ structure [50]. High-resolution Na 1 s spectra in Na-$K_2Ti_6O_{13}$/BiOI (II) with a prominent peak at 1069.9 eV indicating the presence of Na^+ in the composite [51]. Moreover, the binding energies at 617.9 (I $3d_{5/2}$) and 629.4 eV ($3d_{3/2}$) are corresponding to iodine.

3.2.5. Optical properties (UV-DRS and PL study)

The blue light absorption capability of the materials was checked via UV-DRS optical absorption measurements. It is clearly evidenced that bare Na-$K_2Ti_6O_{13}$ did not having absorption in visible region especially in blue region (420–480 nm) (Fig. 6a), besides, it has absorption edge of 360 nm with a calculated optical energy of 3.4 eV by the Kubelka-Munk (K-M) function. It is also evidenced that there is no blue light absorption capability of bare Na-$K_2Ti_6O_{13}$. The prepared Na-$K_2Ti_6O_{13}$/BiOCl (I & II) exhibited a strong visible absorption especially in blue region (420–480 nm) and having absorption edge at 590 nm. The DRS of the Na-$K_2Ti_6O_{13}$/BiOCl (I & II) catalysts represented an absorption choice in the whole visible region, and particularly in blue region of the visible spectrum. With the Na-$K_2Ti_6O_{13}$/BiOCl (II), the absorption choice gradually increased in blue region when compared with Na-$K_2Ti_6O_{13}$/BiOCl (I). Both materials have good blue light absorption, thus active under blue LED. Here, BiOCl catalyst was decorated on Na-$K_2Ti_6O_{13}$ rod, for efficient e^- and h^+ separation under Blue LED illumination. The Kubelka-Munk (K.M) method was used for measurements of bandgap energy.

$$F(R)E^{1/2} = \left[\frac{(1-R)^2}{2R} \times h\nu\right]^{1/2} \quad (2)$$

The bandgap energy (Eg) of bare BiOI, bare Na-$K_2Ti_6O_{13}$, and Na-$K_2Ti_6O_{13}$/BiOCl (I & II) were calculated from above eqn (F(R) = K.M function; $h\nu$ –energy of incident photon), and the DRS and bandgap energy of BiOCl discussion comes later in degradation mechanism section. The bandgap energies of Na-$K_2Ti_6O_{13}$, Na-$K_2Ti_6O_{13}$/BiOCl (I), Na-$K_2Ti_6O_{13}$/BiOCl (II) and BiOI were 3.48, 3.41, 3.40 and 1.89 eV, respectively (Fig. 6 c-f). The band gap energy of these materials Na-$K_2Ti_6O_{13}$/BiOCl (I), Na-$K_2Ti_6O_{13}$/BiOCl (II)) were calculated via base and fitted lines correction [52], the band gap energy estimation obtained by intersection of the two fitting lines. Following combination of BiOCl with Na-$K_2Ti_6O_{13}$, the absorption behaviour of Na-$K_2Ti_6O_{13}$ was extended, and redshifted towards visible regions, especially in blue region. The close contact between BiOCl and Na-$K_2Ti_6O_{13}$ to form a visible active

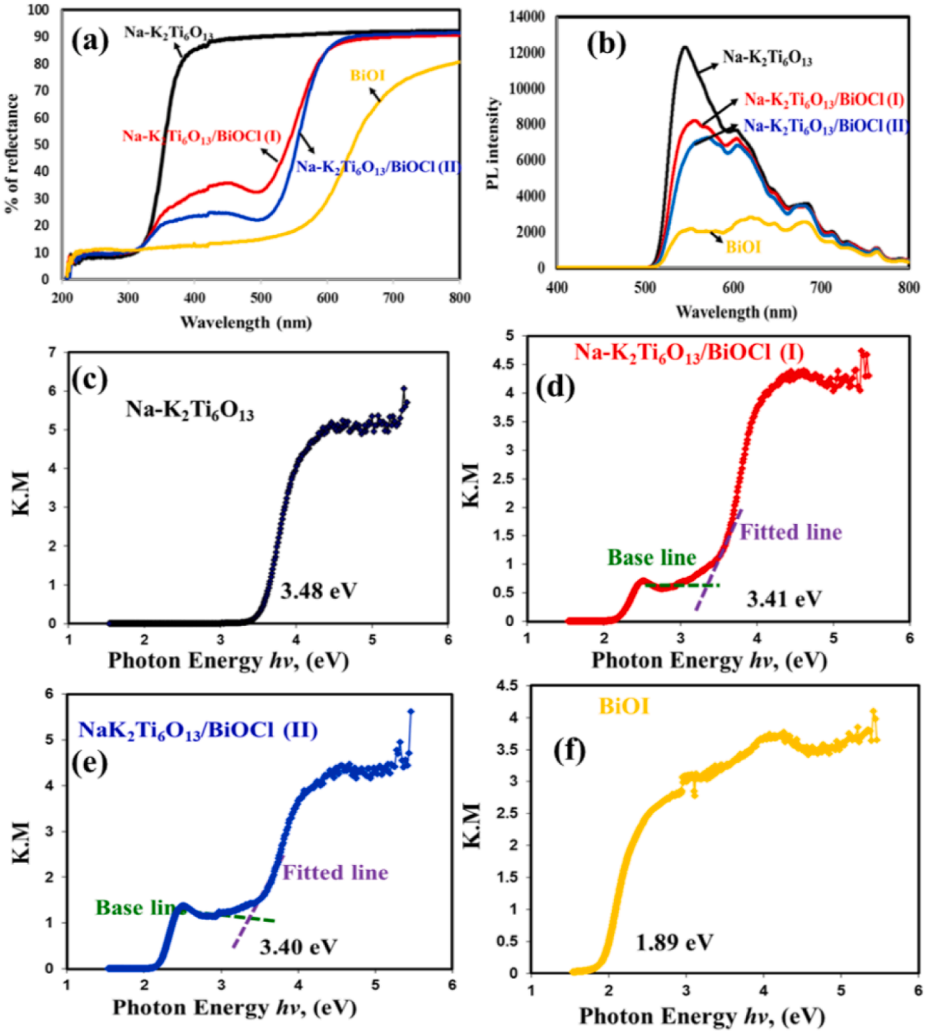

Fig. 6. DRS (a), PL (b) and K.M plots (c-f) of prepared materials.

composite materials for effective environmental remediation. Although there was no blue light absorption capability in Na-$K_2Ti_6O_{13}$, the addition of BiOCl catalyst that intermingled each other, and increase the visible light absorption over a broad range of visible spectrum especially in blue region thus enhanced photocatalytic degradation efficiency under Blue LED. When compare the blue light absorption capability of Na-$K_2Ti_6O_{13}$/BiOCl (I) with Na-$K_2Ti_6O_{13}$/BiOCl (II) catalyst, there is an enhancement in the absorbance in the blue region observed with the increase in the content of BiOCl. However, this combination did not affect the bandgap of the composites significantly.

PL study was made to determine the electron-hole recombination behaviour of the individual semiconductors and mixed composites, and the results depicted in Fig. 6b. The recombination of e^-–h^+ pairs and charge separation (interfacial) are the key factors that affect the fluorescence intensity. Generally, the maximum fluorescence intensity caused by fast electron-hole recombination which results less photocatalytic performance. A strong emission was observed in blue-green region (500–600 nm), and the Na-$K_2Ti_6O_{13}$/BiOCl (I & II) composites exhibit a significant decreased PL emission peak intensity compared to those of bare Na-$K_2Ti_6O_{13}$. The decrease in PL intensity may be attributed to the charge migration between BiOCl and Na-$K_2Ti_6O_{13}$, and it reveals that these two components increase the life time of electron–hole pairs. This suppression of PL intensity indirectly revels that the rate of electron–hole recombination in the composite decreased, and leading to higher photoactivity of the Na-$K_2Ti_6O_{13}$/BiOCl (II).

3.2.6. BET analysis

The surface area of bare Na-$K_2Ti_6O_{13}$ and Na-$K_2Ti_6O_{13}$/BiOCl (II) was determined, and N_2 adsorption – desorption isotherms of Na-$K_2Ti_6O_{13}$ and Na-$K_2Ti_6O_{13}$/BiOCl (II) are presented in Fig. S4 and along with pore size distribution. The isotherms of Na-$K_2Ti_6O_{13}$ and Na-$K_2Ti_6O_{13}$/BiOCl (II) reveal a type II hysteresis loop. The BET surface and pore volume of Na-$K_2Ti_6O_{13}$ and Na-$K_2Ti_6O_{13}$/BiOCl (II) are given in Table S2. Although the BET surface area of Na-$K_2Ti_6O_{13}$/BiOCl (II) (2.98 $m^2\ g^{-1}$) is lower than bare Na-$K_2Ti_6O_{13}$ (15.28 $m^2\ g^{-1}$), the blue light activity of Na-$K_2Ti_6O_{13}$/BiOCl (II) is higher than bare Na-$K_2Ti_6O_{13}$. The pore volume of the Na-$K_2Ti_6O_{13}$/BiOCl (II) is less than that of bare Na-$K_2Ti_6O_{13}$, and this may be due to pores are occupied by BiOCl.

3.3. Photodegradation of TCN

3.3.1. TCN degradation under Blue & White LEDs and solar light

In the tetracycline family tetracycline (TCN) is the most basic compound, and which has been commonly used for human's life. At the same time which may cause serious health problem when the excessive usage of TCN happened. Furthermore, it is uneasy to degrade or remove the excessive TCN. It has been noted that only 15 to 20 % of TCN can be adsorbed, and the remaining 80 % directly released through feces and urine to further cause water and environmental pollution [6,53]. To versatile the activity of the synthesized Na-$K_2Ti_6O_{13}$/BiOCl (II), TCN degradation was carried out under Blue, White LEDs and direct Sun light and the results are depicted in Fig. 7a and S5a, and clearly shows that the irradiation time increases the.

degradation of TCN is also increased in all the processes. About 30 % TCN adsorbed on the surface of the catalyst under dark condition. At 120 min of irradiation, about 68.1, 65.9 and 53.7 % degradation, respectively for White & Blue LEDs and solar light Fig. 7a, and corresponding C_t/C_o values are given in Fig. S5a. The order of activity was found to be White LED > Blue LED > solar light. As per the DRS measurements, Na-$K_2Ti_6O_{13}$/BiOCl has high absorption in visible region, and especially in blue region. The activity of the materials is slightly high in White LED when compared with Blue LED, and less activity in solar light. This may be explained by the following reason. Among the different process, solar process showed minor photocatalytic activity.

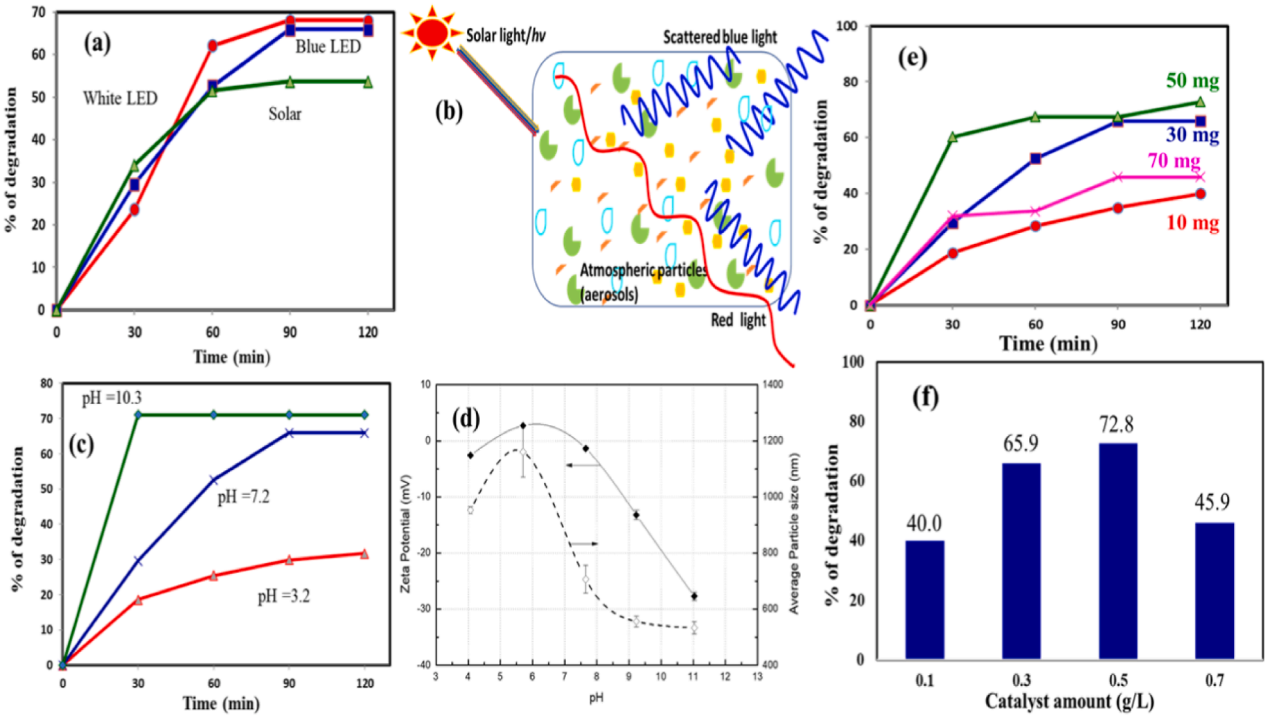

Fig. 7. Photodegradation of TCN (a)[1] Blue, White LEDs and solar light; (b) Blue region of solar light scattered by aerosols; (c)[2] Effect of initial pH on TCN degradation; (d) zeta potential and particle size distribution of Na-$K_2Ti_6O_{13}$/BiOCl (II); (e)[3] Effect of catalyst loading on TCN degradation under Blue LED and (f)[3] corresponding degradation at 120 min; [1] catalyst suspended = Na-$K_2Ti_6O_{13}$/BiOCl (II) (0.3 g/L), pH = 7.2, [TCN] = 20 ppm/100 mL, Blue LED = 5 mW/cm^2, White LED = 46 mW/cm^2; solar light = 95 mW/cm^2; [2] catalyst suspended = Na-$K_2Ti_6O_{13}$/BiOCl (II) (0.3 g/L) Blue LED = 5 mW/cm^2, [TCN] = 20 ppm/100 mL; [3] catalyst suspended = Na-$K_2Ti_6O_{13}$/BiOCl (II); pH = 7.2; Blue LED = 5 mW/cm^2, [TCN] = 20 ppm/100 mL. (For interpretation of the references to colour in this figure legend, the reader is referred to the web version of this article.)

Although solar light containing 47 % of visible region, 46 % infra-red region and 7 % of UV region, the scattering of incident light was happened especially in blue region (440 to 475 nm) of the light by wavelength similar to the size of the particles in the atmosphere (Fig. 7b), and red light has a wavelength (625 to 700 nm) that is larger than most particles thus unaffected [54]. It is expected that most of the blue light in solar spectrum was scattered and leads to less degradation of TCN by Na-$K_2Ti_6O_{13}$/BiOCl under solar process. However, in the White LED, the degradation efficiency of Na-$K_2Ti_6O_{13}$/BiOCl is slightly higher when comparted with Blue LED, and which may be due to White LED (450 to 570 nm) includes total blue spectrum (440 to 475 nm). These results undoubtedly reveal that the synthesized Na-$K_2Ti_6O_{13}$/BiOCl is highly active under Blue LED.

3.3.2. Effect of initial pH on TCN degradation under Blue LED

The photocatalytic degradation of TCN is highly influenced by the initial pH of the TCN solution, and it has been noted that the pH of the solution affecting the surface charge of the catalyst. The effect of pH on the photoreduction of TCN was studied by three different pH (3.2, 7.2 and 10.3). As illustrated in Fig. 7c, increasing the pH from 3.2 to 10.3 enhanced the rate of degradation from 31.7 % to 71 % at 120 min irradiation, and corresponding kinetic values are shown in Fig. S5b. Although the degradation percentage was slightly high in basic condition (pH = 10.3; 71 %), the rate of degradation becomes constant after 30 min irradiation (Fig. 7c), whereas at pH 7.2, 65.9 % degradation observed at 120 min irradiation, it was constantly increased with respect to time. The order of kinetic values of different pH is 0.0096 min^{-1} (pH = 7.2) > 0.0083 min^{-1} (pH = 10.3) > (0.0030 min^{-1} (pH = 3.2). From this observation, the kinetic value of pH 7.2 is higher when compared with acidic and basic conditions. Moreover, there is a huge shift in absorption maximum of TCN observed at higher pH 10.3 (Fig. S5c) (357 nm to 390 nm), and compared with neutral (Fig. S5d) and acidic condition (Fig. S5e). The absorption shift may be due to formation of coloured intermediates at this pH, and it can be visually observed by the colour of the TCN solution at that pH (in set of Fig. S5c and d). TCN is a pH-sensitive, amphoteric nature with three pKa values (3.3, 7.7 and 9.7). In acidic pH, it exists as cationic and basic pH exists as anionic whereas at neutral pH occurred as zwitterion. Because TCN has multiple functional groups hydroxyl, amide, and keto groups. TCN presents different kinds of species at different pH condition. Under present investigation TCN appeared as cationic (pH < 3.32); zwitterionic (3.32 > pH > 7.78); bivalent anionic (pH > 7.78; i.e., here 10.3). In addition, as presented in Fig. 7d, the influence of pH on the zeta potential and average particle size of the Na-$K_2Ti_6O_{13}$/BiOCl presented. The measurements were made between pH 4.07 and 11.03. The zeta potential of the Na-$K_2Ti_6O_{13}$/BiOCl powder moves from −2.57 to + 2.2 mV for pH values increasing from 4.07 to 5.70, and further increase the pH to 7.65, the zeta potential value again becomes slightly negative (-1.34 mV), and went still negative when the pH reached at 11.03 (–22.7 mV). It is clearly revealed that at pH 7.4 the surface charge of the Na-$K_2Ti_6O_{13}$/BiOCl becomes zero, and the Na-$K_2Ti_6O_{13}$/BiOCl surface becomes + ve in the pH range between 4.8 and 7.4, and it becomes –ve in basic condition. At pH values of 7.2, it is the near isoelectric point of Na-$K_2Ti_6O_{13}$/BiOCl, the Na-$K_2Ti_6O_{13}$/BiOCl composite was slightly positive or almost neutral charged. At this same pH, TCN presented as zwitterionic, so there is a strong interaction between neutral or positively charged surface of the Na-$K_2Ti_6O_{13}$/BiOCl and zwitterionic TCN. So, the TCN degradation was very efficient at this neutral pH (7.2). At highly basic conditions (pH = 10.3) the surface of the Na-$K_2Ti_6O_{13}$/BiOCl becomes –ve, and TCN was also presented as anionic, there was a strong repulsion between the surface of the catalyst and TCN occurred at this basic condition results decrease in degradation or becomes constant after certain period. In highly acidic pH < 3.5, the dissolution of the Na-$K_2Ti_6O_{13}$/BiOCl occurred results decrease in the degradation efficiency. At high pH, the particle agglomeration occurred, the average particle size (estimated by number) shows values of 952 nm and 1161 nm at pH 5.07 and 5.70, respectively. However, at almost in neutral pH 7.65, the average particle size was 707 nm (Fig. 7d).

3.3.3. Effect of catalyst loading, initial concentration of TCN, oxone and inorganic anions on degradation of TCN under Blue LED

The amount of catalyst loading on the degradation TCN under Blue LED was investigated with weights ranging from 10 to 70 mg, and the corresponding results are presented in Fig. 7e and f. The amount of photocatalyst was increased from 10, 30, 50 and 70 mg, the degradation percentages were 40.0, 65.9, 72.8 and 45.9, respectively at the time of 120 min irradiation. By increase the catalyst amount from 0.1 g/L to 0.5 g/L, the degradation percentage was increased from 40.0 % to 72.8 %, and further increase the catalyst amount the degradation percentage was decreased (0.7 g/L – 45.9 %).

The reason for increase the activity up to certain level (0.5 g/L) ascribed to more active site availability and depth penetration of blue light into the reaction medium [3]. However, at concentration of the catalyst (beyond 0.5 g/L), the reverse effect was observed that would scatter the penetration of the light into the reaction mixture thus decrease in the degradation activity. It is very important to keep the low amount of catalyst for economical benefit of industrial effluent treatment. The UV–vis spectra of TCN on different time of irradiation with respect to catalyst loading are shown in Fig. S6. An application point of view, it is very important to study the effect of initial concentration of TCN in degradation process. Fig. 8a and b show the increase the TCN concentration from 10 ppm to 40 ppm, the percentage of degradation decreased with increase the concentration from 20 ppm (72.8 %) to 40 ppm (33.4 %), except 10 ppm, at low concentration (10 ppm), the degradation efficiency was slightly decreased (50 % at 120 min irradiation). The degradation efficiency is related to formation of reactive species such as $^{\bullet}OH$ (hydroxyl radical) and superoxide radical anion ($O_2^{\bullet-}$) under the photocatalytic process and the possibility of formed ROS (reactive oxygen species) reacting with TCN molecules. Moreover, the remaining parameters are same (catalyst dosage of 0.5 g/L; pH-7.2; Blue LED with a wavelength of 420–480 nm and with lamp intensity (5 mW/cm^{-2}) except the initial concentration of the TCN. At higher TCN concentration, the photon entering the reaction medium affected thus decrease degradation efficiency. In contrast, at very low TCN concentration (10 ppm), although the photons entered easily, the reverse effect is observed and may be due to the availability of TCN molecule is less, and thus decrease the degradation percentage. The absorption spectra of the TCN vs different initial concentration at different time of irradiation are shown in Fig.S7.

Potassium peroxymonosulfate ($KHSO_5$) is known as oxone, the most effective oxidant, and has been used in photocatalytic reactions. The oxone can produce two reactive species such as sulfate radical anion ($SO_4^{\bullet-}$) and hydroxyl radical ($^{\bullet}OH$) (Eqn (3)). The formed $SO_4^{\bullet-}$ can produce hydroxyl radical upon reaction with water (Eqn. (4)).

$$HSO_5 \rightarrow SO_4^{\bullet-} + {}^{\bullet}OH;\ E^0 = 1.82\ eV\ vs\ NHE \quad (3)$$

$$SO_4^{\bullet-} + H_2O \rightarrow SO_4^{2-} + {}^{\bullet}OH + H^+;\ E^0 = 2.60\ eV\ vs\ NHE \quad (4)$$

However, it has been observed that addition of different dosage of oxone did not enhance the degradation efficiency of Na-$K_2Ti_6O_{13}$/BiOCl (Fig. 8c and d). Two different concentrations of oxone have been added along with Na-$K_2Ti_6O_{13}$/BiOCl catalyst for TCN degradation, and both concentrations, the degradation efficiency of Na-$K_2Ti_6O_{13}$/BiOCl decreased from 72.8 % to 52 % (0.001 M of oxone) and 51.7 % (0.01 M of oxone). This negative effect can be explained by the formation of less reactive $SO_5^{\bullet-}$, when the formed $SO_4^{\bullet-}$ radicals consumed by the excessive HSO_5- (Eq (5)) [55].

$$HSO_5^- + SO_4^{\bullet-} \rightarrow SO_5^{\bullet-} + SO_4^{2-} + H^+ \quad (5)$$

The effect of inorganic anions [56,57] on the degradation of TCN with Na-$K_2Ti_6O_{13}$/BiOCl under Blue LED was studied and the results are

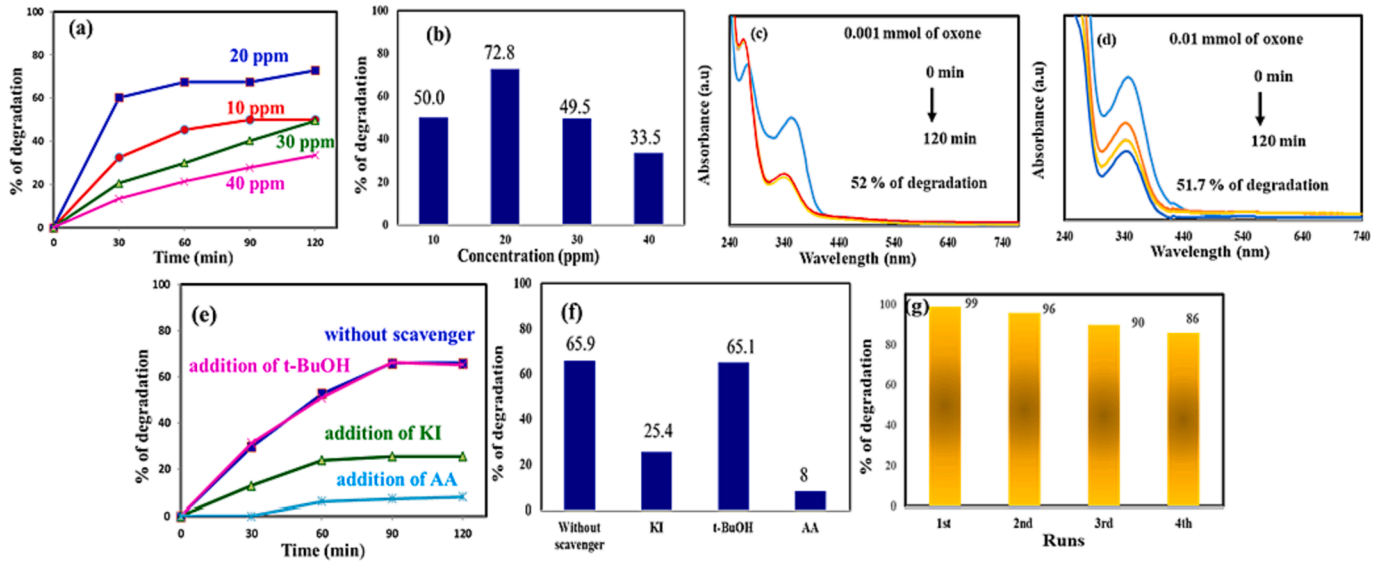

Fig. 8. Effect of initial TCN concentration (a)[1] under Blue LED, (b)[1] corresponding degradation at 120 min, (c and d)[2] Effect of oxone on TCN degradation, (e and f)[3] effect of scavengers on TCN degradation, and (g)[4] Reusability; [1] catalyst suspended = $NaK_2Ti_6O_{13}$/BiOCl (II) (0.5 g/L), pH = 7.2, Blue LED = 5 mW/cm^2; [2]catalyst suspended = $NaK_2Ti_6O_{13}$/BiOCl (II) (0.5 g/L); Blue LED = 5 mW/cm^2, pH = 7.2; [TCN] = 20 ppm/100 mL; [oxone] = 0.01 mmol and 0.001 mmol; [3] catalyst suspended = $NaK_2Ti_6O_{13}$/BiOCl (II) (0.3 g/L), pH = 7.2, Blue LED = 5 mW/cm^2, [scavengers] = 0.1 mmol; [4] catalyst suspended = $NaK_2Ti_6O_{13}$/BiOCl (II) (0.5 g/L), pH = 7.2, [AB 1] = 10 ppm/100 mL, Blue LED = 5 mW/cm^2. (For interpretation of the references to colour in this figure legend, the reader is referred to the web version of this article.)

shown in Table S3. The presence of inorganic anions like carbonate, bicarbonate, sulfate and chloride of sodium salts was significantly decreased the degradation efficiency of the catalyst. The inhibition of these anions is due to their hydroxyl radical scavenging effect [57].

3.3.4. *Radical scavenger's effect, reusability, and comparison with literature*

The formation ROS during photodegradation of TCN with Na-$K_2Ti_6O_{13}$/BiOCl under Blue LED were confirmed by the trapping experiments, and the results are shown in Fig. 8e and f, the corresponding UV–vis spectra of the TCN under different irradiation time are shown in Fig. S8. Without additives, about 65.9 % of degradation observed at 120 min. Three type of additives (0.1 mmol) have been added during the photodegradation experiments along with the catalyst. The addition of potassium iodide (KI), and ascorbic acid (AA) contributes a significant decrease in TCN degradation. KI can scavenge the hole, and observed 25.4 % degradation at 120 min. At the same time addition on AA gave only 8 % degradation, as it scavenges the super oxide radical anions. The $^{\bullet}$OH scavenger TBA gave almost same percentage of degradation (65.1 %). as without scavengers.

The additives react with formed radicals (scavenges the radicals) (eqn 6–8), results decrease in TCN degradation efficiency. At present investigation the most active species involved in the TCN degradation is $O_2^{\bullet-}$ and followed by h^+ [3].

$$A\text{-}H_n\ (AA) + O_2^{\bullet-} \rightarrow A\text{-}H_n\text{–}\ O_2^{\bullet-} \quad (6)$$

$$2\ I^- + 2h^+ \rightarrow I_2 \quad (7)$$

$$R_3C\text{-}OH + {}^{\bullet}OH \rightarrow R_3C\text{-}O^{\bullet} + H_2O \quad (8)$$

The stability of the Na-$K_2Ti_6O_{13}$/BiOCl photocatalyst was tested with cyclic experiments. After each run, the catalyst was collected. After that, the washing was performed with 1:1 (EtOH/H_2O) ethanol/water mixture. After washing, the materials were collected and dried in a hot air oven 110 ^{o}C for 2 h, then it has been used for further runs. Fig. 8g shows the photodegradation efficiency of Na-$K_2Ti_6O_{13}$/BiOCl under Blue LED for AB 1 degradation, and found that there was a drop of efficiency observed from 99 to 86 % for fresh catalyst to third run. This reveals that Na-$K_2Ti_6O_{13}$/BiOCl photocatalyst is stable under Blue LED. The literature comparison was made and LED/Visible active photocatalysts towards TCN and AB 1 degradations are listed in Table S4 and Table S5. Although the optimization processes are different, the Na-$K_2Ti_6O_{13}$/BiOCl photocatalyst efficiently degrade the TCN and AB 1 under Blue LED.

3.3.5. *Degradation pathway of TCN and AB 1 dye with Na-$K_2Ti_6O_{13}$/BiOCl under Blue LED*

It is very important to identify the formed intermediates during photodegradation process. Sometimes intermediate products may be more hazardous than starting materials. The photodegradation TCN and AB 1 with Na-$K_2Ti_6O_{13}$/BiOCl under Blue LED were carried out, and the solution obtained by different irradiation time was extracted by the organic solvents and subjected to GC–MS. The obtained GC–MS spectra were analysed, and based on the molecular weight with respect to retention time, and fragmentation pattern, the degradation pathways were proposed and given in Scheme 1 and Scheme 2, respectively for TCN and AB 1 degradations. For TCN degradation, the identified intermediates (8 compounds) with corresponding retention time are given in Table 1. Under Blue LED with Na-$K_2Ti_6O_{13}$/BiOCl, it was expected that the TCN underwent deamidation produced compound **I**, and by tetracene ring opening produced compound **II** and 4-(dimethylamino)-1,4,4a,5,6,8a-hexahydro-3,8,8a-trihydroxy-1-oxonaphthalene-2-carboxamide (**DP1**). Compound I further underwent tetracene ring opening and C—N bond cleavage produced compound **II** and compound **III**. The identified intermediate product **DPI** underwent partial dihydroxylation and C—N cleavage produced 1,4,4a,5,6,8a-hexahydro-3-hydroxy-1-oxonaphthalene-2-carboxamide (**DP2**) with retention time (RT) of 28.7 min. At the same time, compound **2** underwent dehydroxylation, demethylation along with naphthyl ring opening produced 2,3-dimethylphenol (**DP3**) with RT of 29.9 min. **DP3** underwent further degradation produced compound **IV**. Compound **III** underwent further degradation produced naphthyl ring opening product 5-(2-hydroxyallyl)cyclohex-1-enol (**DP4**) and partial dehydroxylation product 4,4a,5,6-tetrahydro-3-hydroxynaphthalen-1(8aH)-one (**DP5**). The identified intermediate **DP2** underwent further degradation is also produced **DP5** and 4,4a,5,6-tetrahydronaphthalen-1(8aH)-one (**DP6**). The identified intermediate

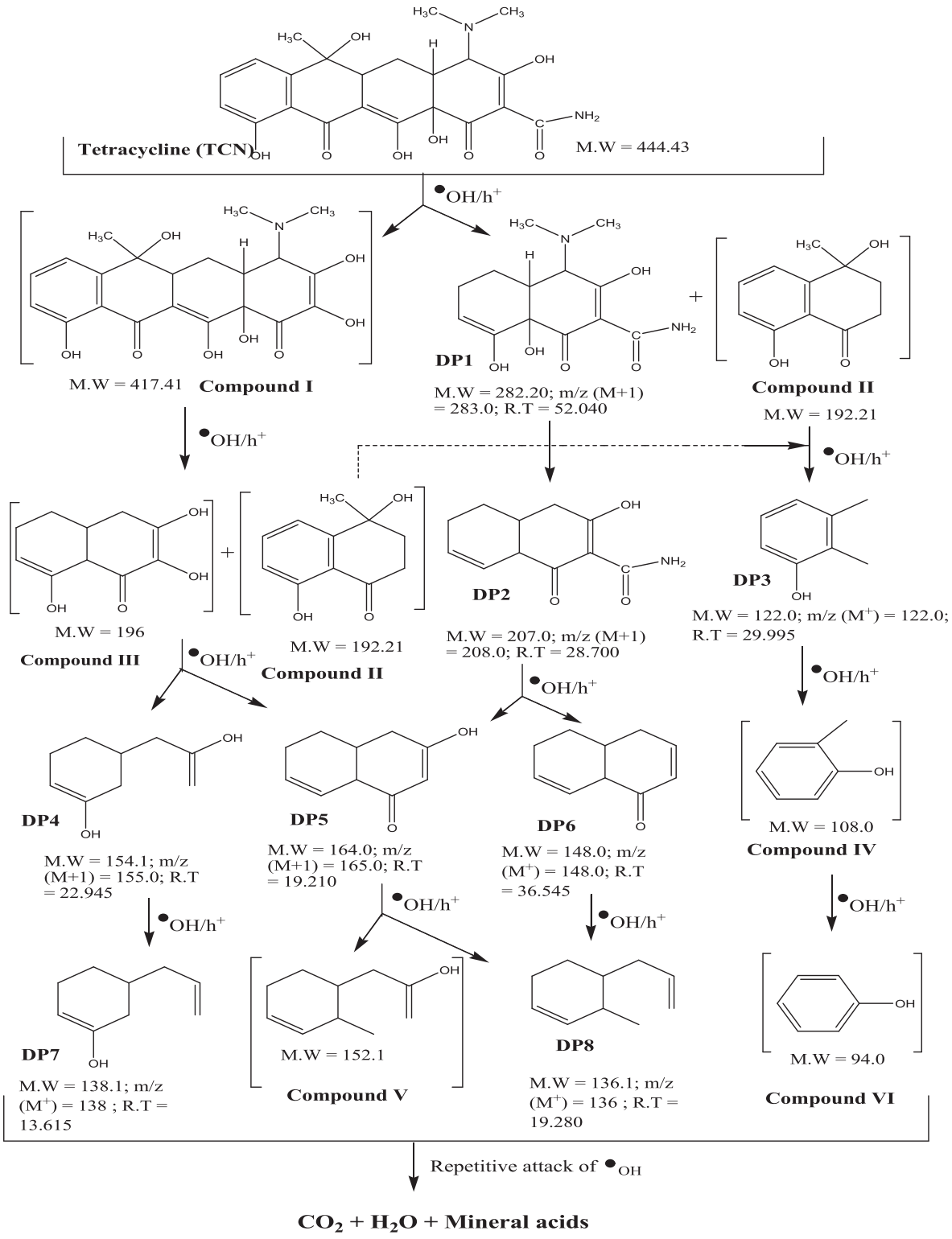

Scheme 1. Proposed degradation pathway of TCN by Na-$K_2Ti_6O_{13}$/BiOCl under Blue LED.

compound DP4 underwent dehydroxylation and produced 5-allylcyclohex-1-enol (**DP7**) with R.T of 13.6 min. The compound **DP5** underwent further degradation produced naphthyl ring opened products compound **V** and 4-allyl-3-methylcyclohex-1-ene (**DP8**). Compound **VI** was formed form compound **IV** via demethylation. Finally, it is predictable that the identified intermediates (**DP7** & **DP8**) and compounds (**V** & **VI**) underwent further degradation to nontoxic products (carbon dioxide, water and mineral acids).

The degradation pathway of AB 1 dye with Na-$K_2Ti_6O_{13}$/BiOCl under Blue LED is proposed in Scheme 2, and intermediates details are given in Table S6. Initially, (7-(2-(4-nitrophenyl)diazenyl)-2-(2-phenyldiazenyl)-8-aminonaphthalene-1,3,6-triol (**DP1**) was formed

from AB 1 dye via desulfonation by hydroxyl groups. The identified intermediate compound **DP1** underwent further degradation and produced 2,7,8-triaminonaphthalene-1,3,6-triol (**DP2**), 4-nitrobenzenamine (**DP3**) and compound **I**. Compound **I** underwent deamination

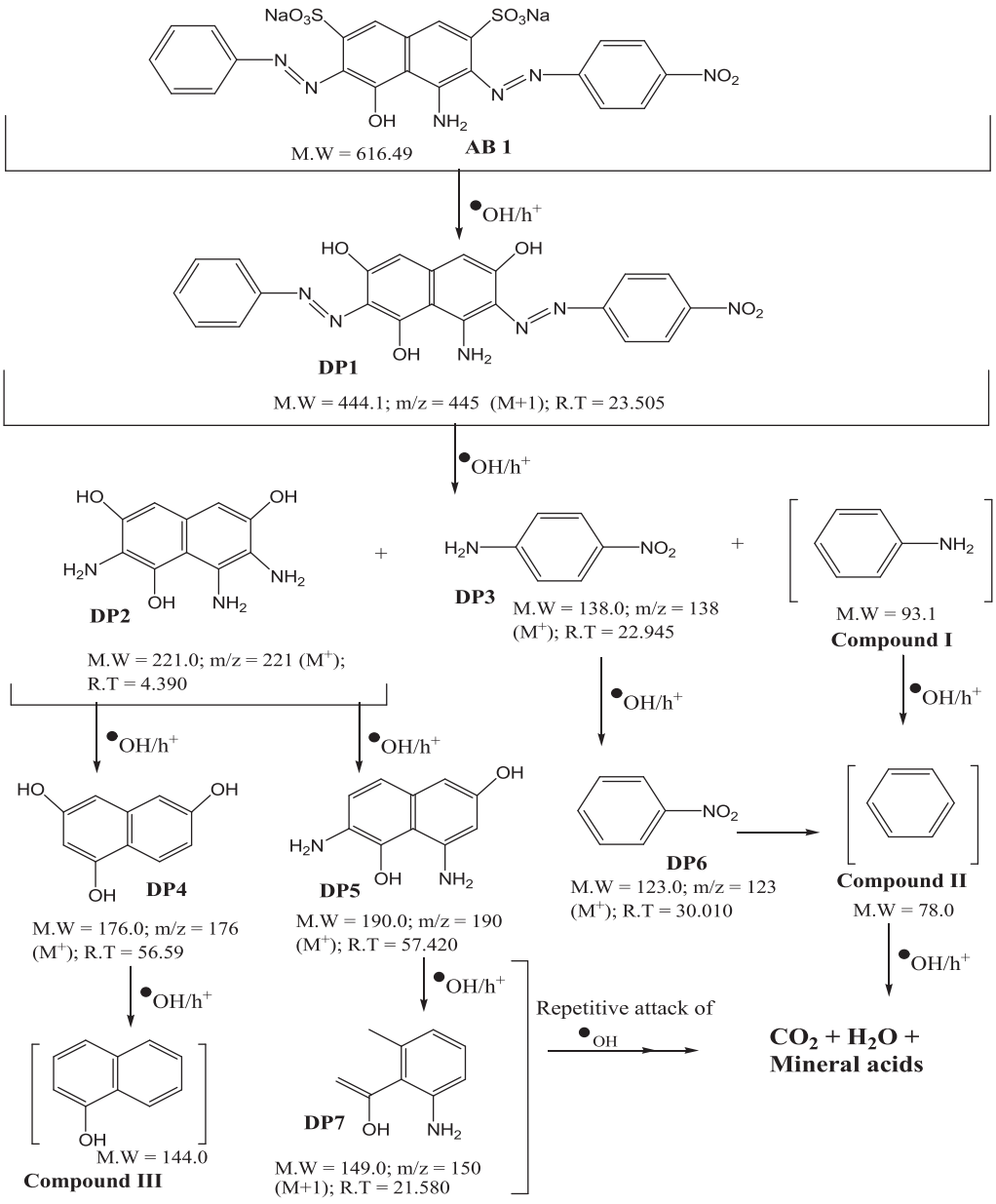

Scheme 2. Proposed degradation pathway of AB 1 dye by Na-$K_2Ti_6O_{13}$/BiOCl under Blue LED.

and produced compound **II**. The identified intermediate compound **DP2** produced naphthalene-1,3,6-triol (**DP4**) via deamination and produced 2,8-diaminonaphthalene-1,6-diol (**DP5**) via partial dihydroxylation. The identified intermediate compound **DP2** produced nitrobenzene (**DP6**) via deamination. The compound **DP4** underwent further degradation produced compound **III**. At the same time, the compound **DP5** underwent naphthyl ring opening and produced 1-(2-amino-6-methylphenyl)ethanol (**DP 7**). The identified intermediate **DP6** is also produced compound **II**. Finally, the identified intermediate **DP7** and compounds (**II & III**) are also going to be mineralized.

3.4. Disinfection of the total coliform bacteria (TC) and multidrug resistant bacteria (MDRB) in wastewater effluent under Blue LED

The synthesized Na-$K_2Ti_6O_{13}$/BiOCl was effectively utilized for tetracycline (TCN) antibiotic and AB 1 degradation under Blue LED. Generally, bacterial disinfection study was performed under UV-A or UV-C light. As we know, especially UV-C light is little harmful than visible light [58,59]. Here, the Blue LED active Na-$K_2Ti_6O_{13}$/BiOCl is used for disinfection of the total coliform bacteria (TC) in real wastewater effluent (ie secondary effluent, SE) and the results are shown in Fig. 9a. There was no significant reduction of TC observed when Na-$K_2Ti_6O_{13}$/BiOCl under dark condition up to 120 min. Under the same condition, the total coliform bacterial cell density decreased significantly with Na-$K_2Ti_6O_{13}$/BiOCl irradiated under Blue LED (Fig. 9a). In specific, Blue LED with Na-$K_2Ti_6O_{13}$/BiOCl inactivated the TC (≈99 % disinfection efficiency) at 120 min. The corresponding plates (2nd dilution) were displayed in Fig. 9b. However, the direct Blue LED irradiation cause significant reduction of CFU in the secondary effluents [60], we have taken multidrug resistant bacteria (MDRB), *Enterobacter asburiae* (SC_1), was isolated from hospital waster, for the inactivation study, and which is also resistant to self-photolysis by Blue LED. Cell viability experiment was conducted to test the activity of the Na-$K_2Ti_6O_{13}$/BiOCl in Blue LED irradiation and the results are depicted in Fig. 9c. The initial concentration of *Enterobacter asburiae* (SC_1) was 1.88 × 10^8 CFU/mL in dark condition (bacterial suspension with nanocomposite) which shows no change even at 120 min. Also, there is no log reduction observed in Blue LED light condition without Na-$K_2Ti_6O_{13}$/

Table 1
Mass spectral data of identified intermediates during degradation of TCN by Na-$K_2Ti_6O_{13}$/BiOCl (II) under Blue LED.

S. No	Compounds	Name of the compound	Retention Time (min)	m/e values
1	**DP1** ($C_{13}H_{18}N_2O_5$)	4-(dimethylamino)-1,4,4a,5,6,8a-hexahydro-3,8,8a-trihydroxy-1-oxonaphthalene-2-carboxamide	52.040	**283** (**M + 1**), 212, 199, 188, 171, 152, 129, 112, 98, 84, 71, 57, 43, 42, 27.
2	**DP2** ($C_{11}H_{13}NO_3$)	1,4,4a,5,6,8a-hexahydro-3-hydroxy-1-oxonaphthalene-2-carboxamide	28.700	**208** (**M + 1**), 120, 115, 107, 94, 77, 71, 55, 43, 39, 27, 15
3	**DP3** ($C_8H_{10}O$)	2,3-dimethylphenol	29.995	**122** (**M^+**), 110, 95, 85, 83, 78, 69, 60, 55, 41, 29
4	**DP4** ($C_9H_{14}O_2$)	5-(2-hydroxyallyl)cyclohex-1-enol	22.945	**155** (**M + 1**), 138, 123, 110, 95, 82, 80, 67, 57, 54, 43, 41, 31, 29
5	**DP5** ($C_{10}H_{12}O_2$)	4,4a,5,6-tetrahydro-3-hydroxynaphthalen-1(8aH)-one	19.210	**165** (**M + 1**), 149, 135, 124, 122, 105, 97, 91, 84, 77, 74, 65, 55, 51, 43.
6	**DP6** ($C_{10}H_{12}O$)	4,4a,5,6-tetrahydronaphthalen-1(8aH)-one	36.545	**148** (**M^+**), 115, 105, 85, 77, 62, 51, 43, 37, 27.
7	**DP7** ($C_9H_{14}O$)	5-allylcyclohex-1-enol	13.615	**138** (**M^+**), 123, 107, 96, 81, 77, 67, 65, 53, 43, 41, 27.
8	**DP8** ($C_{10}H_{16}$)	4-allyl-3-methylcyclohex-1-ene	19.280	**136** (**M^+**), 122, 105, 94, 85, 63, 51, 39, 26

BiOCl (Fig. 9c). In contrast, there is substantial reduction (1.2 log, initial 1.88×10^8 CFU/mL to 0.166×10^8 CFU/mL) in bacteria concentration observed under Blue LED light irradiation with Na-$K_2Ti_6O_{13}$/BiOCl. Therefore, this Na-$K_2Ti_6O_{13}$/BiOCl can effectively control (90 % reduction) the growth of Blue light resistant MDR bacteria under Blue LED light irradiation.

3.5. TCN, AB 1 degradation mechanism and microbial activity of Na-$K_2Ti_6O_{13}$/BiOCl under Blue LED

The formation of heterostructure between Na-$K_2Ti_6O_{13}$ and BiOCl along with trace amount of BiOI was confirmed by XPS measurements, a suitable mechanism is proposed based on the energy levels of these components (Scheme 3). Appling electronegativity Mulliken theory, valence band (VB) ($E_{VB} = E_{CB} + E_g$) and conduction band ($E_{CB} = X - Ec - (1/2)\ E_g$) edges were estimated [28]. E_C represents the energy of free electron (4.5 eV, hydrogen scale) and DRS measurements provide the bandgap of the material (E_g), and X represents electronegativity of the material and calculated from electron affinity and first ionization energy of the atom, $X = 1/2\ (E_{EA} + E_{ion})$. For applying those values, the positive E_{VB} position were obtained for Na-$K_2Ti_6O_{13}$ and BiOCl, and are + 2.24 eV and + 2.56 eV, respectively. The corresponding E_{CB} edges were calculated to be –1.24 eV and –0.64 eV. To form a heterojunction structure between Na-$K_2Ti_6O_{13}$ and BiOCl, the electrons would be transferred from Na-$K_2Ti_6O_{13}$ to BiOCl because the CB position of Na-$K_2Ti_6O_{13}$ was more negative than that of BiOCl. However, the Na-$K_2Ti_6O_{13}$/ BiOCl is irradiated by Blue LED, the BiOCl is excited more when compared with Na-$K_2Ti_6O_{13}$ (there was no significant percentage of dye degradation (AB 1) was observed with Na-$K_2Ti_6O_{13}$ under Blue LED), since BiOCl absorbs more blue light (about 72 % decolorization observed when BiOCl was used as photocatalyst for AB 1 degradation under Blue LED) as observed in DRS measurements (see the Na-$K_2Ti_6O_{13}$/BiOCl composites DRS, and BiOCl was prepared separately [5], and corresponding DRS and KM plot were given in Fig. S9). Although the pure BiOCl has the band gap energy of 3.3 eV, it shows entire visible absorption (see Fig. S9). Moreover, the visible light absorption of composites (Na-$K_2Ti_6O_{13}$/BiOCl-I & II) (see Fig. 6) many folds increases when compared with pristine Na-$K_2Ti_6O_{13}$ (see Fig. 6). It has been noticed that, in the composites, BiOI phase also presented in little amount (confirmed by XPS measurements) along with BiOCl. So, the presence of BiOX (BiOCl/BiOI (trace) mixture) in the composites (Na-$K_2Ti_6O_{13}$/BiOCl-I & II) enhances the visible absorption (especially in blue region) of the materials and make these catalysts active under Blue LED. The analysis about the band structures of Na-$K_2Ti_6O_{13}$ and BiOCl could give us more information about the charge separation by the Blue LED, and transfer during photocatalysis. Along with BiOCl, BiOI also participate in a minor role in the mechanism, the E_{VB} and E_{CB} edges of BiOI were estimated to be + 2.375 eV and + 0.485 eV, respectively. Although the CB edge of BiOI is not suitable for superoxide radical anion production, it has been believed that the narrow bang gap behaviour BiOI, the electrons present in the VB of BiOI can also further go to higher positions at − 2.06 eV, particularly under visible light (>400 nm) [28]. DRS measurements confirm that BiOI has efficient blue light absorbance property, accordingly thus the new transformed CB edge potentials of BiOI (−2.06 eV) can fit with BiOCl, and there is a possibility of electron jump from CB of BiOI to that of BiOCl, and then respond with O_2 produced highly reactive ROS (superoxide radical anion).

From the above analysis, we could find that the charge transfer would not follow the heterojunction because most of the excited electrons are present in CB of BiOCl, and which position is less negative than active Na-$K_2Ti_6O_{13}$. Therefore, we proposed internal charge allocation of the prepared Na-$K_2Ti_6O_{13}$/BiOCl composite system. In this case, the e^- in CB of BiOCl would combine with h^+ in VB of Na-$K_2Ti_6O_{13}$, left the separated e^- in CB of Na-$K_2Ti_6O_{13}$ and h^+ left in VB of BiOCl, and making charge separation more efficient. The electrons react with dissolved oxygen and holes react with water produced highly reactive oxygen species ROS. Both species are very efficient towards TCN and AB 1 degradation. The formed ROS cause cell death for TC and MDR bacteria [30,61,62]. The formed ROS were confirmed by trapping experiments and discussed in the previous sections, and super oxide radical anion played a major role in the degradation followed by holes.

4. Conclusions

In the globalization era, water pollution, and wastewater disposal are a major problem. To find the solution for the treatment of wastewater, and to reduce its harmful effect towards human health as well as in the environment, is a major part of current research scenario in the world-wide. Na-$K_2Ti_6O_{13}$/ BiOCl composites were prepared by two step process, initially Na-$K_2Ti_6O_{13}$ was synthesized using the molten salt method, BiOCl was added via solid state dispersion cum precipitation method. Almost 99 % AB 1 degradation observed with $K_2Ti_6O_{13}$/BiOCl (II) under Blue LED. This composite was effectively utilized for antibiotic TCN degradation under Blue & White LEDs and solar light, and found that Na-$K_2Ti_6O_{13}$/BiOCl effectively degrade TCN under Blue LED than solar light, and comparable with White LED. The surface, structural and morphology properties of the synthesized materials obtained via XRD, FT-IR, FE-SEM, HR-TEM, Elemental mapping, EDS, XPS, PL, DRS and BET. XRD and elemental mapping clearly show that the formation of

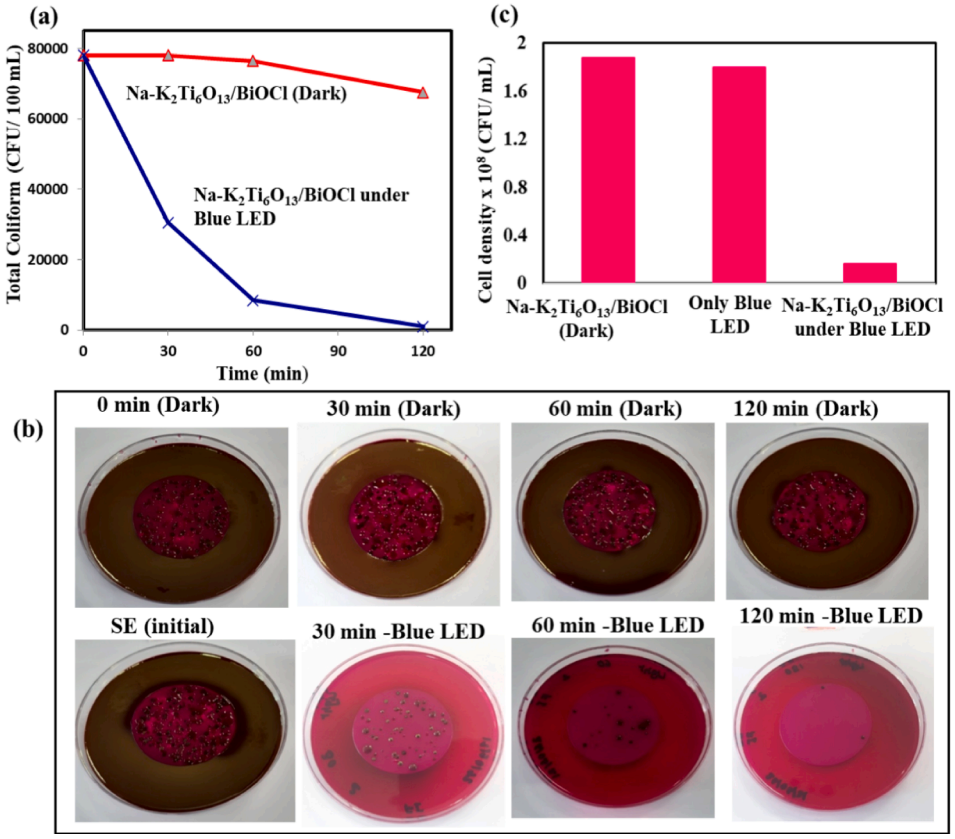

Fig. 9. The disinfection of TC in SE by Na-$K_2Ti_6O_{13}$/BiOCl under Blue LED (a and b), corresponding plates (2nd dilution) (b), and (c) disinfection of MDR bacteria *Enterobacter asburiae* (SC_1) in SE by Na-$K_2Ti_6O_{13}$/BiOCl under Blue LED at 120 min irradiation. (For interpretation of the references to colour in this figure legend, the reader is referred to the web version of this article.)

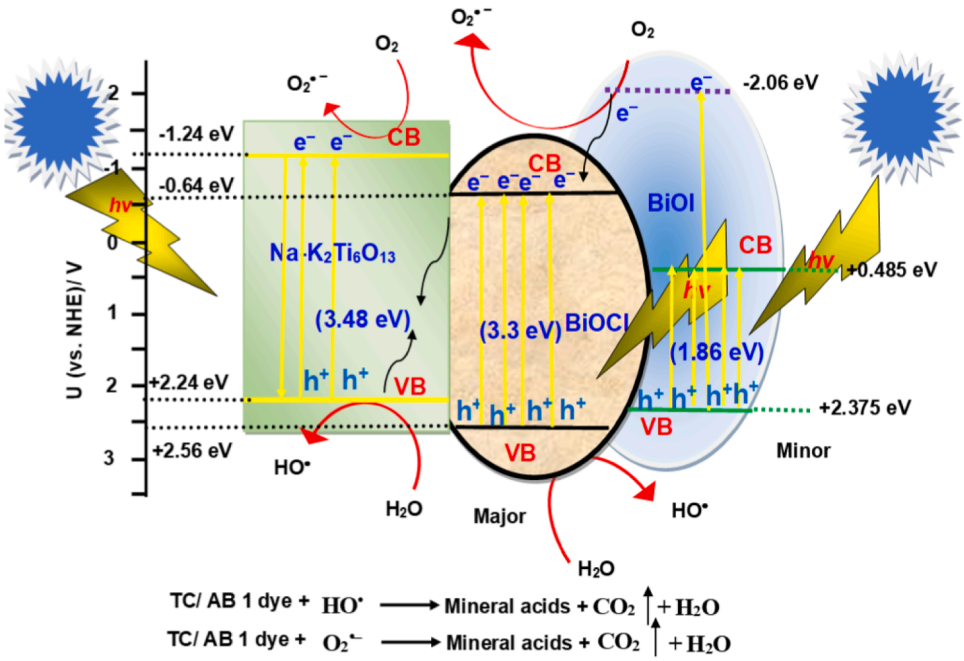

Scheme 3. Proposed degradation mechanism for TCB, AB 1 dye, disinfection of TC and MDR bacteria by Na-$K_2Ti_6O_{13}$/BiOCl under Blue LED.

$K_2Ti_6O_{13}$/BiOCl rather $K_2Ti_6O_{13}$/BiOI. Although iodine present in the composite, and it was not in the form of BiOI (only trace). The three different pH of TCN solution with $K_2Ti_6O_{13}$/BiOCl taken, and the degradation was performed under Blue LED, and reported that pH 7.2 was the ideal pH for efficient removal of TCN, and this was confirmed with kinetic study and the reason was discussed via zeta potential

measurements. The optimum amount catalyst for efficient removal of TCN under Blue LED is found to be 0.5 g/L. Increase the initial concentration of TCN from 20 ppm to 40 ppm, decrease the degradation percentage. Suitable degradation pathways were proposed for TCN, and AB 1 degradations with $K_2Ti_6O_{13}$/BiOCl under Blue LED based on the intermediates formed during reaction by GC–MS analysis. There are eight (**DP1-DP8**) and seven (**DP1-DP7**) possible intermediates were identified by GC–MS analysis for TCN and AB 1 degradations, respectively. The $K_2Ti_6O_{13}$/BiOCl was effectively utilized for SE treatment under Blue LED, and found that it effectively kill the TC and MDR bacteria *Enterobacter asburiae* (SC_1). A suitable mechanism of degradation by $K_2Ti_6O_{13}$/BiOCl under Blue LED was proposed. The formed ROS species were confirmed by scavenging experiments, and the addition of AA retard the reaction significantly, and proven that superoxide radical anions ($O_2^{\bullet-}$) play a vital role in the degradation. Factors such as improved photocatalytic activity of the material under Blue LED, greater blue light absorption capability, and stability of $K_2Ti_6O_{13}$/BiOCl are auspicious in development catalytic support towards energy and environmental applications.

Declaration of Competing Interest

The authors declare that they have no known competing financial interests or personal relationships that could have appeared to influence the work reported in this paper.

Data availability

No data was used for the research described in the article.

Acknowledgments

This Research was supported by the Basic Science Research Program through the National Research Foundation of Korea funded by the Ministry of Education (2020R1I1A305481611). Dr. Krishnakumar Balu would like to thank the Ministry of Universities and the Recovery, Transformation and Resilience Plan from the Spanish government for the "María Zambrano grant 2021" by the Europen Union - NextGenerationEU.

Author contribution: Krishnakumar Balu: Materials synthesis, characterization, photocatalytic experiments and writing first draft. **E. Chicardi**: Software, data curation, and XRD discussion. **R. Sepúlveda**: Software, writing-review, XPS, and FT-IR discussion. **Mani Durai**: Conceptualization, methodology, and editing. **Fahmida Ishaque**: Microbial activity experiment and discussion. **Deepak Chauhan**: Microbial activity experiment. **Young-Ho Ahn**: Conceptualization and supervision.

Electronic supplementary information (ESI) available. GC-MS sample procedure, Figs. S1-S9, Scheme S1, and Tables S1-S6 are given in this section.

Appendix A. Supplementary data

Supplementary data to this article can be found online at https://doi.org/10.1016/j.seppur.2022.122998.

References

[1] J. You, Y. Guo, R. Guo, X. Liu, A review of visible light-active photocatalysts for water disinfection: Features and prospect, Chem. Eng. J. 373 (2019) 624–641.
[2] T. Lia, C. Wang, T. Wang, L. Zhu, Highly efficient photocatalytic degradation toward perfluorooctanoic acid by bromine doped BiOI with high exposure of (001) facet, Appl. Catal. B. 268 (2020), 118442.
[3] S. Ravikumar, D. Mani, M.R. Khan, N. Ahmad, S. Sylvestre, C. Surya, B. Krishnakumar, V. Pandiyan, Young-Ho Ahn, Ag-TiO_2@Pd/C nanocomposites for efficient degradation of Reactive Red 120 dye and ofloxacin antibiotic under UV and solar light and its antimicrobial activity, J. Environ. Chem. Eng. 9 (2021), 106657.
[4] R. Dadigala, R. Bandi, M. Alle, C.W. Park, S.Y. Han, G.J. Kwon, S.H. Lee, Effective fabrication of cellulose nanofibrils supported Pd nanoparticles as a novel nanozyme with peroxidase and oxidase-like activities for efficient dye degradation, J. Hazard. Mater. 436 (2022), 129165.
[5] D. Mani, C. Deepak, D. Mathivanan, S. Mathavan, K. Sakthivel, E. Elangovan, Y. H. Ahn, Layered KTO/BiOCl nanostructures for the efficient visible light photocatalytic degradation of harmful dyes, Chemosphere 306 (2022), 135659.
[6] Z. Zhu, R. Yang, C. Zhu, C. Hu, B. Liu, Novel Cu-Fe/LDH@$BiOI_{1.5}$ photocatalyst effectively degrades tetracycline under visible light irradiation, Adv Powder Technol, 32 (2021) 2311–2321.
[7] X. Song, Y. Wang, T. Zhu, J. Liu, S. Zhang, Facile synthesis a novel core–shell amino functionalized MIL-125(Ti) micro-photocatalyst for enhanced degradation of tetracycline hydrochloride under visible light, Chem. Eng. J. 416 (2021), 129126.
[8] J. Guo, L. Wang, X. Wei, Z.A. Alothman, M.D. Albaqami, V. Malgras, Y. Yamauchi, Y. Kang, M. Wang, W. Guan, X. Xu, Direct Z-scheme $CuInS_2/Bi_2MoO_6$ heterostructure for enhanced photocatalytic degradation of tetracycline under visible light, J. Hazard. Mater. 415 (2021), 125591.
[9] K. Zhou, Y. Liu, J. Hao, One-pot hydrothermal synthesis of dual Z-scheme BiOBr/g-C_3N_4/Bi_2WO_6 and photocatalytic degradation of tetracycline under visible light, Mater. Lett. 281 (2020), 128463.
[10] X. Zheng, Y. Liu, X. Liu, Q. Li, Y. Zheng, A novel PVDF-TiO_2@g-C_3N_4 composite electrospun fiber for efficient photocatalytic degradation of tetracycline under visible light irradiation, Ecotoxicol. Environ. Saf. 210 (2021), 111866.
[11] T. Guo, L. Jiang, H. Huang, Y. Li, X. Wu, G. Zhang, Enhanced degradation of tetracycline in water over Cu-doped hematite nanoplates by peroxymonosulfate activation under visible light irradiation, J. Hazard. Mater. 416 (2021), 125838.
[12] P. Hemmati-Eslamlu, A. Habibi-Yangjeh, S. Asadzadeh-Khaneghah, H. Chand, V. Krishnan, Integration g-C_3N_4 nanotubes and Sb_2MoO_6 nanoparticles: Impressive photoactivity for tetracycline degradation, Cr (VI) reduction, and organic dyes removals under visible light, Adv Powder Technol 32 (2021) 2322–2335.
[13] Y. Ma, M. Li, J. Jiang, T. Li, X. Wang, Y. Song, S. Dong, In-situ prepared MIL-53 (Fe)/BiOI photocatalyst for efficient degradation of tetracycline under visible-light driven photo-Fenton system: Investigation of performance and mechanism, J. Alloys Compd 870 (2021), 159524.
[14] S. Ni, Z. Fu, L. Li, M. Ma, Y. Liu, Step-scheme heterojunction g-C_3N_4/TiO_2 for efficient photocatalytic degradation of tetracycline hydrochloride under UV light, Colloids Surf. A Physicochem. Eng. Asp. 649 (2022), 129475.
[15] U. Ghosh, A. Majumdar, A. Pal, 3D macroporous architecture of self-assembled defect-engineered ultrathin g-C3N4 nanosheets for tetracycline degradation under LED light irradiation, Mater. Res. Bull. 133 (2021), 111074.
[16] S. Li, M. Cai, Y. Liu, C. Wang, K. Lv, X. Chen, S-Scheme photocatalyst TaON/Bi_2WO_6 nanofibers with oxygen vacancies for efficient abatement of antibiotics and Cr(VI): Intermediate eco-toxicity analysis and mechanistic insights, Chinese, J. Catal. 43 (2022) 2652–2664.
[17] S. Li, M. Cai, Y. Liu, C. Wang, R. Yan, X. Chen, Constructing $Cd_{0.5}Zn_{0.5}S/Bi_2WO_6$ S-scheme heterojunction for boosted photocatalytic antibiotic oxidation and Cr(VI) reduction, Adv Powder Mater. 2 (2023), 100073.
[18] M. Cai, Y. Liu, C. Wang, W. Lin, S. Li, Novel $Cd_{0.5}Zn_{0.5}S/Bi_2MoO_6$ S-scheme heterojunction for boosting the photodegradation of antibiotic enrofloxacin: Degradation pathway, mechanism and toxicity assessment, Sep. Purif. Technol. 304 (2023), 122401.
[19] C. Wang, S. Li, M. Cai, R. Yan, K. Dong, J. Zhang, Y. Liu, Rationally designed tetra (4-carboxyphenyl) porphyrin/graphene quantum dots/bismuth molybdate Z-scheme heterojunction for tetracycline degradation and Cr(VI) reduction: Performance, mechanism, intermediate toxicity appraisement, J. Colloid Interface Sci. 619 (2022) 307–321.
[20] A. khan, U. Alam, D. Ali, D. Bahnemann, M. Muneer, Surface modification of Na-$K_2Ti_6O_{13}$ photocatalyst with Cu(II)- nanocluster for efficient visible-light-driven photocatalytic activity, Mater. Lett. 220 (2018) 50–53.
[21] L.F. Garay-Rodríguez, L.M. Torres-Martínez, E. Moctezuma, Photocatalytic performance of $K_2Ti_6O_{13}$ whiskers to H_2 evolution and CO_2 photo-reduction, J. Energy Chem. 37 (2019) 18–28.
[22] Q. Wang, S. Guan, B. Li, 2D graphitic-C_3N_4 hybridized with 1D flux-grown Na-modified $K_2Ti_6O_{13}$ nanobelts for enhanced simulated sunlight and visible-light photocatalytic performance, Catal, Sci. Technol. 7 (2017) 4064–4078.
[23] N. Song, Y. Liu, B. Liu, Y. Liu, Y. Tan, W. Wei, T. Luo, Controlled synthesis of platy potassium titanates from potassium magnesium titanate, RSC Adv. 3 (2013) 8326–8330.
[24] X. Zhu, A. Yamamoto, H. Yoshida, Alkali hexatitanate photocatalysts with various morphologies for selective reduction of carbon dioxide with water, Dalton Trans. 50 (2021) 7976–7983.
[25] K.K. Somashekharappa, S. Venkatesh Lokesh, Hydrothermal Synthesis of $K_2Ti_6O_{13}$ Nanotubes/Nanoparticles: A Photodegradation Study on Methylene Blue and Rhodamine B Dyes, ACS, Omega 6 (2021) 7248–7256.
[26] P. Ponce-Peña, M. Poisot, A. Rodríguez-Pulido, M.A. González-Lozano, Crystalline Structure, Synthesis, Properties and Applications of Potassium Hexatitanate: A Review, Materials 12 (2019) 4132.
[27] Y. Guan, W. Liu, S. Zuo, X. Yan, J. Ni, C. Yao, F. Wu, Effect of Sb doping on the photocatalytic performance of Z-scheme TiO_2NRA/SnO_2/potassium titanate heterojunction and its photocatalytic mechanism, Mater Sci Semicond Process 131 (2021), 105849.
[28] B. Krishnakumar, R. Hariharan, V. Pandiyan, A. Aguiar, A.J.F.N. Sobral, Gelatin-assisted g-TiO_2/BiOI Heterostructure Nanocomposites for Azo Dye Degradation under Visible Light, J. Environ Chem. Eng. 6 (2018) 4282–4288.

[29] APHA, Standard methods for the examination of water and wastewater, 21st edn. American Public Health Association/ American Water Works Association/Water Environment Federation, 2005, Washington DC, USA.
[30] R.K. Manoharan, P. Gangadaran, S. Ayyaru, B.C. Ahn, Y.H. Ahn, Self-healing functionalization of sulfonated hafnium oxide and copper oxide nanocomposite for effective biocidal control of multidrug-resistant bacteria, New J Chem 45 (2021) 9506–9517.
[31] Q. Wang, Q. Guo, B. Li, Low temperature synthesis and characterization of the substitutional Na-modified $K_2Ti_6O_{13}$ nanobelts with improved photocatalytic activity under UV irradiation, RSC Adv. 5 (2015) 66086.
[32] X. Ji, S. Wu, S. Zhang, X. Zhao, Study on the Reaction Mechanism of Potassium Titanate Fibers, Integrated Ferroelectrics 153 (2014) 156–163.
[33] Y. Mi, M. Zhou, L. Wen, H. Zhao, Y. Lei, A highly efficient visible-light driven photocatalyst: two dimensional square-like bismuth oxyiodine nanosheets, Dalton Trans. 43 (2014) 9549–9556.
[34] Q. Geng, H. Xie, Y. He, Y. Sun, X. Hou, Z. Wang, F. Dong, Atomic interfacial structure and charge transfer mechanism on in-situ formed BiOI/$Bi_2O_2SO_4$ p–n heterojunctions with highly promoted photocatalysis, Appl. Catal. B. 297 (2021), 120492.
[35] Q. Li, J. Ren, Y.J. Hao, Y.L. Li, X.J. Wang, Y. Liu, R. Su, F.T. Li, Insight into reactive species-dependent photocatalytic toluene mineralization and deactivation pathways via modifying hydroxyl groups and oxygen vacancies on BiOCl, Appl. Catal. B. 317 (2022), 121761.
[36] X. Jia, J. Cao, H. Lin, M. Zhang, X. Guo, S. Chen, Transforming type-I to type-II heterostructure photocatalyst via energy band engineering: A case study of I-BiOCl/I-BiOBr, Appl. Catal. B. 204 (2017) 505–514.
[37] M. Cai, Y. Liu, K. Dong, C. Wang, S. Li, novel S-scheme heterojunction of $Cd_{0.5}Zn_{0.5}S$/BiOCl with oxygen defects for antibiotic norfloxacin photodegradation: Performance, mechanism, and intermediates toxicity evaluation, J. Colloid Interface Sci. 629 (2023) 276–286.
[38] S. Li, M. Cai, C. Wang, Y. Liu, N. Li, P. Zhang, X. Li, Rationally designed Ta_3N_5/BiOCl S-scheme heterojunction with oxygen vacancies for elimination of tetracycline antibiotic and Cr(VI): Performance, toxicity evaluation and mechanism insight, J. Mater. Sci. Technol. 123 (2022) 177–190.
[39] T.B. Li, G. Chen, C. Zhou, Z.Y. Shen, R.C. Jin, J.X. Sun, New photocatalyst BiOCl/BiOI composites with highly enhanced visible light photocatalytic performances, Dalton Trans. 40 (2011) 6751–6758.
[40] S. Sehati, M.H. Entezari, Ultrasound facilitates the synthesis of potassium hexatitanate and co-intercalation with PbS–CdS nanoparticles, Ultrason Sonochem 32 (2016) 348–356.
[41] W. Tang, Y. Zhang, H. Guo, Y. Liu, Heterogeneous activation of peroxymonosulfate for bisphenol AF degradation with $BiOI_{0.5}Cl_{0.5}$, RSC Adv. 9 (2019) 14060.
[42] A. Yousefi, A. Nezamzadeh-Ejhieh, Characterization of BiOCl/BiOI binary catalyst and its photocatalytic activity towards rifampin, J. Photochem. Photobiol. A 433 (2022), 114135.
[43] B.M. Reddy, B. Chowdhury, P.G. Smirniotis, An XPS study of the dispersion of MoO_3 on TiO_2–ZrO_2, TiO_2–SiO_2, TiO_2–Al_2O_3, SiO_2–ZrO_2, and SiO_2–TiO_2–ZrO_2 mixed oxides, Appl. Catal., A 211 (2001) 19–30.
[44] Q. Teng, X. Zhou, B. Jin, J. Luo, X. Xu, H. Guan, W. Wang, F. Yang, Synthesis and enhanced photocatalytic activity of a BiOI/TiO_2 nanobelt array for methyl orange degradation under visible light irradiation, RSC Adv. 6 (2016) 36881–36887.
[45] M. Gao, H. Liang, S. Bao, T. Xu, Y. Zhang, J. Bai, C. Li, Bifunctional BiOCl/TiO_2 decorated membrane for antibiotic photodegradation and oil-water emulsion separation, Appl. Surf. Sci. 578 (2022), 151960.
[46] A. Shoja, A. Habibi-Yangjeh, M. Mousavi, S. Ghosh, BiOBr and BiOCl decorated on TiO_2 QDs: Impressively increased photocatalytic performance for the degradation of pollutants under visible light, Adv Powder Technol 31 (2020) 3582–3596.
[47] J. Hou, K. Jiang, M. Shen, R. Wei, X. Wu, F. Idrees, C. Cao, Micro and nano hierachical structures of BiOI/activated carbon for efcient visible-lightphotocatalytic reactions, Sci Rep 7 (2017) 11665.
[48] J. Han, G. Zhu, M. Hojamberdiev, J. Peng, X. Zhang, Y. Liu, B. Gea, P. Liua, Rapid adsorption and photocatalytic activity for Rhodamine B and Cr(VI) by ultrathin BiOI nanosheets with highly exposed 001 facets, New J. Chem. 39 (2015) 1874.
[49] X. Xu, Q. Sun, Y. Ma, X. Jiang, N. Niu, L. Chen, Synthesis of KCl-doped lignin carbon dots nanoenzymes for colorimetric sensing glutathione in human serum, Sens. Actuators B Chem. 364 (2022), 131881.
[50] Q. Wang, Z. Guo, J.S. Chung, Formation and structural characterization of potassium titanates and the potassium ion exchange property, Mater. Res. Bull. 44 (2009) 1973–1977.
[51] R. Ruben Maça, V. Etacheri, Effect of Vinylene Carbonate Electrolyte Additive on the Surface Chemistry and Pseudocapacitive Sodium-Ion Storage of TiO_2 Nanosheet Anodes, Batteries 7 (2021) 1.
[52] P. Makuła, M. Pacia, W. Macyk, How to correctly determine the band gap energy of modified semiconductor photocatalysts based on UV−Vis Spectra, J. Phys. Chem. Lett. 9 (2018) 6814–6817.
[53] S. Li, M. Cai, Y. Liu, J. Zhang, C. Wang, S. Zang, Y. Li, P. Zhang, X. Li, In situ construction of a C_3N_5 nanosheet/Bi2WO6 nanodot S-scheme heterojunction with enhanced structural defects for the efficient photocatalytic removal of tetracycline and Cr(VI), Inorg. Chem. Front. 9 (2022) 2479–2497.
[54] C. Gueymard, SMARTS2: a simple model of the atmospheric radiative transfer of sunshine: algorithms and performance assessment. Florida Solar Energy Center Cocoa, FL, 1995 (https://www.pveducation.org/pvcdrom/properties-of-sunlight/atmospheric-effects).
[55] Y.R. Wang, W. Chu, degradation of 2,4,5-trichlorophenoxyacetic acid by a novel Electro-Fe(II)/Oxone process using iron sheet as the sacrificial anode, Water Res. 45 (2011) 3883–3889.
[56] S. Li, C. Wang, M. Cai, Y. Liu, K. Dong, J. Zhang, Designing oxygen vacancy mediated bismuth molybdate (Bi_2MoO_6)/*N*-rich carbon nitride (C3N5) S-scheme heterojunctions for boosted photocatalytic removal of tetracycline antibiotic and Cr(VI): Intermediate toxicity and mechanism insight, J. Colloid Interface Sci. 624 (2022) 219–232.
[57] B. Krishnakumar, M. Swaminathan, Photodegradation of Acid Violet 7 with AgBr–ZnO under highly alkaline conditions, Spectrochim Acta A Mol Biomol Spectrosc 99 (2012) 160–165.
[58] M. Belloli, M. Cigarini, G. Milesi, P. Mutti, E. Berni, Effectiveness of two UV-C light-emitting diodes (LED) systems in inactivating fungal conidia on polyethylene terephthalate, Innov Food Sci Emerg Technol 79 (2022), 103050.
[59] O. Mitxelena-Iribarren, B. Mondragon, E. Lorenzo, C. Smerdou, F. Guillen-Grima, J. E. Sierra-Garcia, F. Rodriguez-Merino, S. Arana, Evaluation of the degradation of materials by exposure to germicide UV-C light through colorimetry, tensile strength and surface microstructure analyses, Mater. Today Commun. 31 (2022), 103690.
[60] R. K. Manoharan , C. J. Raorane , F. Ishaque , Y.H, Ahn, Antimicrobial photodynamic inactivation of wastewater microorganisms by halogenated indole derivative capped zinc oxide, Environ. Res., 214 (2022) 113905.
[61] Y. Zhang, C. Lin, Q. Lin, Y. Jin, Y. Wang, Z. Zhang, H. Lin, J. Long, X. Wang, CuI-BiOI/Cu film for enhanced photo-induced charge separation and visible light antibacterial activity, Appl. Catal. B. 235 (2018) 238–245.
[62] V. Rodríguez-González, S. Obregón, O.A. Patrón-Soberano, C. Terashima, A. Fujishima, An approach to the photocatalytic mechanism in the TiO_2-nanomaterials microorganism interface for the control of infectious processes, Appl. Catal. B. 270 (2020), 118853.